ADVANCES OF HIGH-ORDER INTERACTIONS IN THE HUMAN BRAIN: APPLICATIONS IN AGING AND NEURODEGENERATION

Thesis
for obtaining the PhD degree in Biophysics and Computational Biology of Science Department, Universidad de Valparaíso

Thesis
for obtaining the PhD degree in Biomedical Research Program, University of Basque Country

Marilyn Gatica Briceño

Advisors:
Dr. Patricio Orio
Dr. Jesús M. Cortés

"I am never so happy as when I am really engaged in good earnest, & it makes me must wonderfully cheerful & merry at other times, which is curious & very satisfactory"
Ada Lovelace, on January 10, 1841.

This work is dedicated to my beloved family, fantastic friends, and a lovely husband. ♡.

Agradecimientos

- A Rodrigo Cofré, Jesús M Cortés, y Patricio Orio. Muchas gracias por su dedicación en este trabajo de tesis, por sus consejos, por su confianza y por su gran motivación. Junto a ustedes he tenido un gran camino de crecimiento académico y personal.
- Pedro Mediano y Fernando Rosas. Muchas gracias por su confianza, por todas las horas de discusión y su increíble motivación en este trabajo de tesis.
- Biocruces Bizkaia Health Research Institute.
- Computational Neuroimaging Lab, BioCruces-Bizkaia Health Research Institute.
- Valparaiso Neural Dynamics Laboratory (VaNDaL).
- Brain Information Complexity Laboratory (Brincolab).
- Centro de Investigación y Modelamiento de Fenómenos Aleatorios Valparaíso (CIMFAV).
- A los profesores que me guiaron en la Universidad de Santiago de Chile, especialmente a Patricio Rojas, Sergio Plaza, Guillermo Sánchez e Ignacio Guerra.
- CONICYT-PFCHA/Doctorado Nacional/2019-21190577, 2019-2022.
- Beca de Doctorado FIB-UV, 2018.

Contents

List of Figures

List of Tables

Abstract

The human brain generates a large repertoire of spatio-temporal patterns, which support a wide variety of motor, cognitive, and behavioral functions. The most accepted hypothesis in modern neuroscience is that each of these representations is encoded in different brain networks. From MRI, networks can be defined anatomically ("structural connectivity"-SC) or functionally ("functional connectivity"-FC). Interestingly, while SC is by definition pairwise (white matter fibers project from one region to another), FC is not. In this thesis we have focused on the study of high-order interactions (HOI) that occur in functional networks, beyond the existing statistical relationships in pairs of regions. When evaluating the interacting n-plets, from triplets to order n, a novel type of statistical interdependencies appear, namely the synergistic and redundant interactions, which are inaccessible when evaluating interacting pairs. The study of these HOI in the human brain in aging and neurodegeneration is the purpose of this thesis. Starting from the O-Information formalism, we have systematically analyzed synergistic and redundant interactions in functional networks of the human brain. In the first part of this thesis, we have applied this formalism to the aging brain and have found a higher prevalence of redundant interdependences in older participants compared to younger ones, and this effect occurs in all orders of interaction within regions located in the prefrontal and motor areas, thus involving working memory, motor and executive functions. In the second part of the thesis, we have built a neurobiological-realistic computational model of the whole-brain that incorporates SC and FC data. Our model shows that, related to aging, variations in functional patterns can be explained by changes in SC, which neurodegenerate as we age. Based on this finding, we propose a simple nonlinear neurodegeneration model that is representative of healthy (non-pathological) aging and that reproduces the age variations that occur in the HOI structure of functional data. Finally, in the last part of this thesis, we have applied our formalism to a clinical population, and in particular to a cohort of older patients with Frontotemporal Dementia (FTD), comparing the redundant and synergistic patterns that occur in the HOI of these brains, in comparison with a control group of healthy population, well matched in age, sex and years of education with the FTD cohort. For this chapter, we have developed a new statistical tool that allows us to detect clusters that are significantly different between groups and where the interaction is predominantly synergistic or redundant. For our particular case of FTD, redundant triplets were found in higher-order vision networks, default mode, and salience network. Similarly, synergistic triplets were found in the primary auditory cortex. Together, the results obtained in this thesis pave an avenue of multiple possibilities in the study of HOI as informational markers in the high-order functionality of the brain, and how its alterations could reveal new organizational aspects of the human brain in health and disease.

1

Introduction

1.1 Healthy aging and brain diseases

The study of aging from the perspective of neuroscience is of great importance from a socio-economic point of view, as the number of older people is increasing dramatically worldwide. Projections suggest that the percentage of people aged 60 or older will increase from 900 million in 2015 to 2.1 billion in 2050 [1, 2]. Aging is a major risk factor for late-onset brain disorders that accelerate cognitive and motor decline and worsen the quality of life.

Several causes of systemic decline –across multiple scales– underlie the process of aging, involving biological, cognitive and psychosocial effects. For example, aging disrupts circadian rhythms and sleep cycles [3], resulting in poor sleep quality, impair cognitive performance such as information processing speed, working memory, executive functions, and reasoning [4], and increases mental health issues including anxiety and depression [5].

In addition, it is important for many reasons to characterise the underlying cognitive changes when a healthy brain age, and to distinguish between chronological brain age and and the brain age estimated from the magnetic resonance imaging data of patients. First, this could help inform targeted care and treatment. Second, aging is a significant risk factor for neurodegenerative diseases that impair cognition, such as Alzheimer's disease and Parkinson's disease. Fortunately, advances in neuroimaging, data preprocessing and machine learning have synergistically contributed to producing better solutions to the problem of age prediction. [6].

These advances, leading to a deeper understanding of the healthy aging process, could motivate new interventions or protective therapies against age-related deterioration or neurodegenerative diseases [7, 8, 9, 10, 11].

1.2 Neuroimaging

Several non-invasive neuroimaging techniques exist to measure brain activity in humans. Magnetic resonance imaging (MRI) is a versatile technology for extracting very different functional and structural information of the brain organization on a large scale. There are many acquisition parameters in MRI, such as the intensity of the magnetic field with which we interact, its direction, shape, and the number of pulse sequences for changing magnetic gradients or their relaxation times. In particular, structural MRI allows the study of anatomical tissues such as gray and withe matter, cerebrospinal fluid (CSF) along the whole-brain including cortical, subcortical and deep structures such as the brain stem or the striatum [12]. Diffusion magnetic resonance imaging (dMRI) allows tracking the random 3D motion of water molecules in these tissues. This is relevant because in gray matter and cerebrospinal fluid, for example, diffusion is highly isotropic; while in white matter water molecules diffusion becomes highly anisotropic, with some directions being more visited than others. After some computational strategies for tracking reconstruction, dMRI provides a map of white matter tracts connecting pairwise of regions within the entire brain at the millimeter resolution.

Functional magnetic resonance imaging (fMRI) is a non-invasive imaging technique discovered in the early 90's by Seiji Ogawa [13]. This technique relies on the magnetic properties of blood, in particular, the in-and-out oxygenation cycles of hemoglobin in blood. The normal diamagnetic oxyhemoglobin which not interacts with the magnetic field becomes after oxygen consumption paramagnetic, increasing the signal contrast, which receives the name of blood-oxygen level dependent (BOLD). The main hypothesis on which fMRI relies is that if brain areas are somehow implicated in a specific task, they will demand sustained neuronal activity, increasing oxygen consumption. In this way, and very importantly, fMRI is an indirect measure of neuronal activity.

Neuroimaging advances in data acquisition have evolved hand in hand with innovation and progress in image processing methodologies and tools [14, 15, 16, 17]. There are several software and toolbox to preprocess and clean artifacts from the different MRI modalities, such as FSL, ANTs, MRtrix3, SPM, AFNI, to name a few. It is important to mention that these new neuroimaging techniques and preprocessing tools are leading to great progress in quantitative clinical research.

Other techniques for whole brain neuronal activity are electroencephalography (EEG) or magnetoencephalography (MEG), both of which rely on the electrical and magnetic properties of the cellular excitability of brain cells. Although EEG and MEG have a very good temporal resolution, even capable of capturing milliseconds neuronal activity variations, their spatial localization is poor. In this PhD thesis, we will focus on the MRI modalities of fMRI and dMRI.

1.3 Structural connectivity

Several effects of aging on quantitative brain structural imaging have been described. Along the lifespan, the total brain volume increases from childhood to adolescence by approximately 25% on average, remains constant for the three following decades, and finally decays back to childhood size at late ages [18]. Additionally, it has been shown that the amount of atrophy in aged brains is not homogeneous, as some anatomical regions are more affected than others: well-known aging-targeted structures are the hippocampus [19], prefrontal cortex [20] and basal ganglia [21, 22]. White matter degenerates faster than gray matter along the lifespan, indicating that the overall connectivity is diminished with age [23]. Moreover, a progressive decrease in many tract-integrity measures has been shown using diffusion imaging, which is more pronounced in subjects above 60 years of age [7, 24].

Aging has also been studied in terms of an anatomical map of brain neural connections, namely, structural connectivity (SC). Several researchers characterized the SC across the lifespan following the seminal ideas introduced by Tononi, Sporns, and Edelman (Tononi, et al., 1994), which postulate the integration and segregation concepts. The latter enables brain areas to perform specialized tasks independently, whereas the former allows brain areas to work together to perform goal-directed tasks [25, 26]. Remarkably, several studies have described decreasing segregation and increasing integration across a healthy lifespan [27, 28, 29]. However, the relationship between changes in brain structure and function leading to age-related decline remains largely unknown [30, 31, 32, 24].

1.4 Functional connectivity

Another way to quantify age-related changes is to use pairwise functional interdependencies. The functional correlations between two time series of brain activity are quantified typically using the Pearson correlation. Those correlations are stored in a matrix called functional connectivity (FC). Furthermore, several studies go beyond and also analyze the changes of functional connectivity over time [33, 34, 35, 36, 37, 38].

Previous studies of functional connectivity along the lifespan during resting state have shown that regions within the default mode network (DMN) become less functionally connected with age [39, 8, 40, 32]. Additionally, the frontoparietal, dorsal attention, and salience networks also show some degree of age-related decline, including reduced within-network connectivity [41, 42, 43, 39]. In contrast, between-network connectivity increase with age between the DMN, somatosensory, and the frontoparietal control networks. A stronger connectivity between the frontoparietal and dorsal attention networks has been reported as well [41, 44, 31, 45].

Taken together, these findings suggest a general loss of functional specificity or cir-

cuit segregation across brain circuits [46]. Moreover, an increase in between-network interactions is a dominant feature of aging brains. Albeit important progress in our understanding of the effects of aging on brain function, these effects are less understood than the effects on structural connectivity, which shows progressive age-related disconnection.

1.5 High-order functional interactions

An important limitation of the previously described functional connectivity studies is that their analysis is restricted to pairwise FC, ignoring possible higher order effects called high-order interactions or high-order interdependencies. High-order interdependencies allow us to characterize the brain pattern organization, distinguishing redundancy- and synergy-dominated interactions that play crucial roles in neural dynamics [47, 48, 49, 50, 51, 52]. Redundancy is understood here as an extension of the conventional notion of the correlation between more than two variables, in which each variable has "copy" of some common information shared with other variables [53]. By contrast, synergy corresponds to statistical relationships that regulate the whole but not the parts [54, 55, 56]. Synergy allows local independence and global cohesion to coexist, a condition that is instrumental for higher order brain functions, while redundancy – including highly synchronized situations like deep sleep or epileptic seizures – would make brains less well-suited to this [26, 57].
A pioneer study of high-order interactions and aging showed significant changes in the synergies and redundancies of triple interactions over the individual's lifespan [58], as well as a redundant role of the default mode network (DMN). However, the effects of aging on interactions beyond triple relationships remain largely unexplored to the best of our knowledge. This motivated our first thesis work.

1.6 Hypothesis and objectives

1.6.1 Hypothesis

"Functional redundancy and synergy are informational markers that describe the lifespan changes in a healthy brain. Moreover, the variations in these functional higher-order informational organizations could be explained by the changes of the brain's anatomical networks, which degenerate as we age. Differences in synergy and redundancy could differentiate healthy brains with pathological neurodegenerative brains."

1.6.2 Objectives

- To quantify the brain changes in the higher-order functional interdependences across the lifespan in terms of redundancy and synergy, using fMRI data from

participants between 10 to 80 years.

- To analyze if the variations in the high-order functional interdependences could be led by the changes in the brain's anatomical networks across the lifespan, using a Dynamic mean field whole-brain modeling (DMF).

- To quanitfy the changes in the high-order functional interdependencies produced by Frontotemporal Dementia.

1.7 Overview

This work is divided into five chapters:
Ch1. Introduction: We provide an overview of the PhD thesis, outline the research topic and review the relevant literature for the development of this thesis.
Ch2. Materials and Methods: We introduce the main tools and strategies used in the development of this thesis, including the global methodology used in this research. We relate these methods to broader literature in this research field. Beyond the general methodological scenario, the following three chapters have their specific methods.
Ch3. High-order in the aging brain: We investigate how the higher- order informational organization of the brain changes with age. We hypothesize that redundancy and synergy are informational markers to describe the healthy lifespan changes in brain activity. Our results show that older participants (from 60 to 80 years old) exhibit higher predominance of redundant dependencies than younger participants. This effect is evident for all interaction orders.
Ch4. High-order interdependencies in a whole-brain model: We combine functional and diffusion MRI data with a Dynamic mean field whole-brain modeling (DMF) to investigate the mechanisms underlying age variations in the structure and high-order functional interactions. We hypothesize that the variations in functional patterns can be explained by the changes of the brain's anatomical networks, which degenerate as we age. The DMF model successfully reproduces the increased redundancy-dominated interdependencies of BOLD activity across brain areas in the older participants, and across all interaction orders, in agreement with observations in chapter 3.
Ch5. High-order interactions applied to Frontotemporal Dementia: We analyzed high-order interactions applied to Frontotemporal Dementia. We hypothesize that redundancy and synergy are informational markers to describe the changes in brain activity produced by Frontotemporal Dementia. Our third result shows a clustering of triplets with unbalanced synergy and redundancy and with some regions participating only in redundant or synergistic triplets.

2

Materials and Methods

2.1 Information Theory

2.1.1 Shannon entropy

Definition 1 *The* **entropy** *of a discrete random variable X with a probability mass function $p(x)$ is defined by:*

$$H(X) = -\sum_{x} p(x) \log\left(p(x)\right).$$

Remarks:

- The entropy will be measured in bits if using the logarithm to base 2 or nats using the natural logarithm.
- The entropy of X can also be interpreted as the expected value of the random variable $\log(1/p(X))$.

2.1.2 Differential entropy

Definition 2 *The* **differential entropy** *of a continuous random variable X with PDF $f(x)$ is defined as:*

$$H(X) = -\int_{\chi} f(x) \log\left(f(x)\right) dx,$$

where χ is the support of f.
The differential entropy is sometimes written as $H(f)$ rather than $H(X)$.

Definition 3 *Let X be a random variable normally distributed with mean μ and standard deviation σ, denoted by $X \sim N(\mu, \sigma^2)$, then the differential entropy in nats of X is defined by:*

$$H(X) = \ln\left(\sigma\sqrt{2\,\pi\,e}\right).$$

2.1.3 Mutual information

The Mutual Information (I) is an extension of Shannon entropy for two random variables, which quantify the information shared by two random variables, X and Y, and is defined by:

$$\mathrm{I}(X,Y) = H(X) + H(Y) - H(X,Y),$$

where $H(X), H(Y)$ are the marginal entropies, and $H(X,Y)$ is the joint entropy of X, and Y. Mutual Information is a non-negative and symmetric quantity.

2.1.4 Interaction Information

The Interaction Information (II) is a generalization of the Mutual Information for three or more random variables. We focus on the case of three random variables due to the II sign has a relevant interpretation. If $\mathrm{II} > 0$ the interaction is redundancy-predominated, and $\mathrm{II} < 0$ correspond to synergy-dominated value. Mathematically, for any three random variables X, Y, Z,

$$\begin{aligned}
\mathrm{II}(X,Y,Z) &= \mathrm{I}(X,Y) - \mathrm{I}(X,Y|Z), \\
&= H(X) + H(Y) - H(X,Y) - (H(X,Z) + H(Y,Z) - H(X,Y,Z) - H(Z)) \\
&= H(X) + H(Y) + H(Z) - (H(X,Y) + H(X,Z) + H(Y,Z)) + H(X,Y,Z),
\end{aligned}$$

where $\mathrm{I}(X,Y|Z)$ represents the the conditional mutual information between X and Y, conditioned to Z, and, $\mathrm{I}(X,Y|Z) = H(X,Z) + H(Y,Z) - H(X,Y,Z) - H(Z)$.
Finally, notice that it does not matter which variable is conditioned in II because it is symmetric.

2.1.5 Total Correlation and Dual Total Correlation

The *total correlation* (TC), and the *dual total correlation* (DTC), are defined by the following formulas:

$$\mathrm{TC}(\boldsymbol{X}^n) = \sum_{i=1}^{n} H(X_i) - H(\boldsymbol{X}^n) \ , \tag{2.1}$$

$$\mathrm{DTC}(\boldsymbol{X}^n) = H(\boldsymbol{X}^n) - \sum_{i=1}^{n} H(X_i \mid \boldsymbol{X}^n_{-i}) \ . \tag{2.2}$$

Here, $H(\cdot)$ represents the Shannon entropy, and $\boldsymbol{X}^n_{-i}$ represents the vector of $n-1$ variables composed by all minus X_i i.e., $(X_1, \ldots, X_{i-1}, X_{i+1}, \ldots, X_n)$. Both TC and DTC are non-negative generalizations of mutual information, meaning they are zero if and only if all variables $X_1, \ldots, X_n$ are statistically independent of one another.

2.1.6 S-information and O-information

The O-information of a set of n random variables $X_n = (X_1, \ldots, X_n)$ is calculated as

$$\Omega\left(X_n\right) = TC\left(X_n\right) - DTC(X_n)$$

while their S-information is

$$\Sigma\left(X_n\right) = TC\left(X_n\right) + DTC(X_n)$$

We estimate the S-information and O-information for all the different subsets of brain modules from three to twenty brain interactions. For each participant we computed the average O-information and S-information in which the module m participate when interacting with other n regions. We denote it by $\Omega_n^m(k)$ and $\Sigma_n^m(k)$ respectively. Analytically,

$$\Omega_n^m(k) = \frac{1}{\mathcal{Z}_n} \sum_{i_1} \cdots \sum_{i_{n-1}} \Omega_{(k)}(X_m, X_{i_1}, \ldots, X_{i_{n-1}}) \ , \tag{2.3}$$

$$\Sigma_n^m(k) = \frac{1}{\mathcal{Z}_n} \sum_{i_1} \cdots \sum_{i_{n-1}} \Sigma_{(k)}(X_m, X_{i_1}, \ldots, X_{i_{n-1}}) \ ., \tag{2.4}$$

Above, k is the participant index and m is the module index, n interaction order, and

$$\mathcal{Z}_n \equiv \binom{M-1}{n-1}$$

is the total number of subsets of size $n-1$ in an atlas of M modules.
Finally, the average O-information of order n is calculated averaging over the M modules.

$$\Omega_n(k) = \frac{1}{M} \sum_{m=1}^{M} \Omega_n^m(k) \ , \tag{2.5}$$

$$\Sigma_n(k) = \frac{1}{M} \sum_{m=1}^{M} \Sigma_n^m(k) \ . \tag{2.6}$$

2.1.7 Redundancy and Synergy

The O-information is a real-valued metric whose sign serves to discriminate between redundant and synergistic groups of random variables: $\Omega > 0$ corresponds to redundancy-dominated interdependencies, and $\Omega < 0$ characterizes synergy-dominated variables. Moreover, the positive and negative values of the O-information are called for simplicity 'redundancy' and 'synergy,' respectively.
Therefore, we split the O-information on positive and negative values using

$$\Omega^+ = \max\{\Omega, 0\} \quad ; \quad \Omega^- = -\min\{\Omega, 0\} \ , \tag{2.7}$$

so that $\Omega = \Omega^+ - \Omega^-$. Using these quantities, we calculated the following proxies for redundancy and synergy per subject k, module m, and interaction order n

$$R_n^m(k) = \frac{1}{\mathcal{N}_{n,m}^+} \sum_{i_1} \cdots \sum_{i_{n-1}} \Omega_{(k)}^+(X_m, X_{i_1}, \ldots, X_{i_{n-1}}) \ , \tag{2.8}$$

$$S_n^m(k) = \frac{1}{\mathcal{N}_{n,m}^-} \sum_{i_1} \cdots \sum_{i_{n-1}} \Omega_{(k)}^-(X_m, X_{i_1}, \ldots, X_{i_{n-1}}) \ , \tag{2.9}$$

where $\mathcal{N}_{n,m}^+$ and $\mathcal{N}_{n,m}^-$ represent the number of n-plets with positive and negative O-information values, respectively.
Finally, the average of the redundancy and synergy over all subjects and modules is calculated as

$$R_n(k) = \frac{1}{M} \sum_{m=1}^{M} R_n^m(k) \ , \tag{2.10}$$

$$S_n(k) = \frac{1}{M} \sum_{m=1}^{M} S_n^m(k) \ . \tag{2.11}$$

2.1.8 Gaussian Copula Estimation

We use Gaussian Copula Estimation to compute the O-information and S-information values. This approach exploits the fact that the Mutual Information does not depend on the marginal distributions and therefore, the different quantities can be conveniently transformed into Gaussian random variables for which efficient parametric estimates of high-order interactions exist [52].

The code to compute the metrics used in this thesis (Redundancy, Synergy, O-information, and S-information) has been made publicly available at `www.github.com/brincolab/High-Order-interactions`.

2.2 Statistical analyses

In this study, we compared the group of older participants (I4) with the combination of the three other groups (I1, I2, I3). Different information-based measures were compared using a non-parametric statistical Wilcoxon rank sum test. When appropriate, significance levels for hypothesis testing were corrected for multiple comparisons by controlling the false discovery rate (FDR) following a standard Benjamini-Hochberg procedure [59].

3

High-order interdependencies in the aging brain

3.1 Introduction and hypothesis

Resting state functional magnetic resonance imaging or functional MRI (fMRI) has shown that aging affects functional connectivity (FC) in extended brain networks, specifically altering anterior and posterior regions like the superior and middle frontal gyrus (MFG), posterior cingulate, middle temporal gyrus and the superior parietal region [8, 60]. Other studies have shown that aging may also alter the FC between several regions, possibly indicating compensation or pathological activation [41, 61, 62, 63].
An important limitation of such FC studies is that their analysis is restricted to pairwise FC, ignoring possible higher order effects. Following recent works [64, 65], we assess high-order interactions (beyond pairwise relations) to distinguish redundancy and synergy dominated interactions in neural dynamics [47, 48, 49, 50, 51, 52]. An initial study of high-order interactions and aging showed significant changes in the synergies and redundancies of triple interactions over the individual's lifespan [58], as well as a redundant role of the default mode network (DMN). However, the effects of aging on interactions beyond triple relationships remain largely unexplored to the best of our knowledge.
Here, we built on our previous studies [58] to examine the effects of aging on higher order interactions in the human brain, paying special attention to the interdependencies between four or more brain regions. We employed the recently proposed *O-information* [54], which can be considered a revised version of the measure of neural complexity proposed previously in the context of Partial Information Decomposition [26, 66]. More specifically, O-information captures the balance between redundancies and synergies in arbitrary sets of variables, thereby extending the properties of the interaction information of three variables to larger sets [67]. Redundancy is understood here as an extension of the conventional notion of the correlation between more than two variables, in which each variable has a "copy" of some common information shared with other variables [53].

An example of extreme redundancy is full synchronization, where the status of one signal allows one to predict the status of any other. By contrast, synergy corresponds to statistical relationships that regulate the whole but not the parts [54, 55, 68]. Synergy allows local independency and global cohesion to coexist, a condition that has been recently found to be instrumental for higher order brain functions [56, 69], while redundancy – including highly synchronized situations like deep sleep stages or epileptic seizures – would make brains less well-suited to this [26, 57].

To investigate how the higher order informational organization of the brain changes with age, we studied synergic and redundant interactions of different orders from fMRI data obtained in the resting state from a cohort of 164 healthy volunteers aged 10 to 80 years old.

This approach is novel for two reasons. From a methodological perspective, we present the first application of higher order statistical interdependencies in aging, beyond triplet interactions, developing a formalism to apply the metrics previously presented to fMRI data [54]. In addition, we investigate how aging alters the higher order interdependencies among different brain regions, as inferred directly from fMRI data. In this way, we obtained novel insights into brain aging, whereby the interdependencies in older participants appear to be more redundancy-dominated than those in younger participants, for all interaction orders. When studying how these effects are distributed topographically we found a "redundancy core" that was composed of brain regions that play key roles in the most redundancy-dominated arrangements for all interaction orders.

3.2 Results

We analysed resting-state fMRI data from 164 healthy participants, measuring S-information and the O-information in order to quantify high-order interactions between brain areas in terms of redundancy and synergy. A methodological sketch is shown in Figure 3.1. Participants were divided in four age groups (I1-I4) as described in Materials and methods.

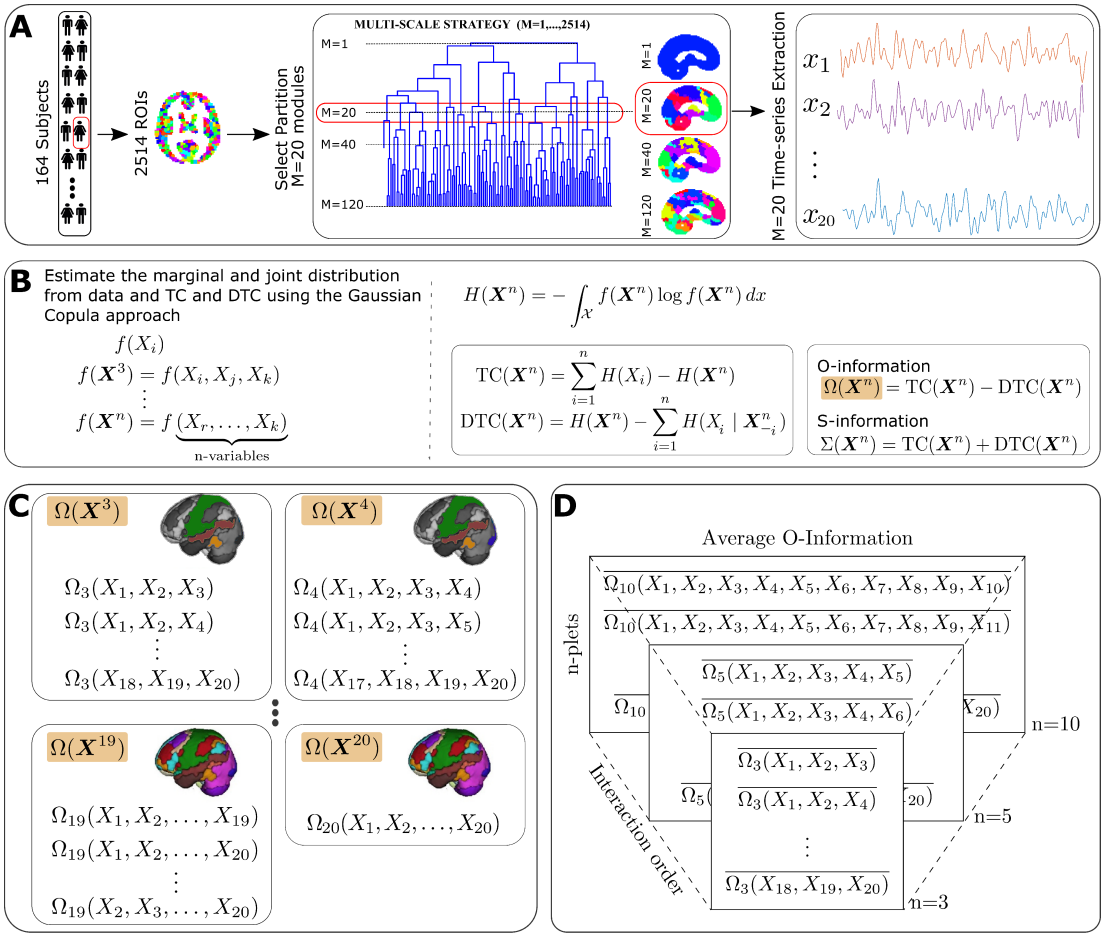

Figure 3.1: **Methodological scheme**. **A)** 164 subjects were included in this study, each represented by 2,514 time series of fMRI signals. Using The Brain Hierarchical Atlas (BHA), the original time series was grouped into M=20 different ones. **B)** The marginal and joint distributions for each subject were estimated from the data using the Gaussian copula, from which the marginal and joint entropies were calculated. Next, the total correlation (TC) and dual total correlation (DTC) were obtained, from which the O- and S-information were finally computed. **C)** For each subject and interaction order, we computed their O-information and S-information values for each n-plet, which were then used for further analyses. **D)** The average O-information values of the participants were also calculated for each n-plet for group-comparisons.

3.2.1 S-information and O-information along lifespan

We first measured the S-information and O-information per age group and interaction order, Figure 3.2 shows that both the S-information and the O-information exhibit significant differences between the old group and the younger ones after correcting with FDR for multiple comparisons. The increase of S-information with age implies an increase of interdependencies between the various brain regions. Interestingly, the increase shown in the older population is significant at all orders, suggesting a widespread effect.

The increase seen in the O-information suggest that the correlations seen in the older population are in general redundancy-dominated, becoming stronger in large orders.

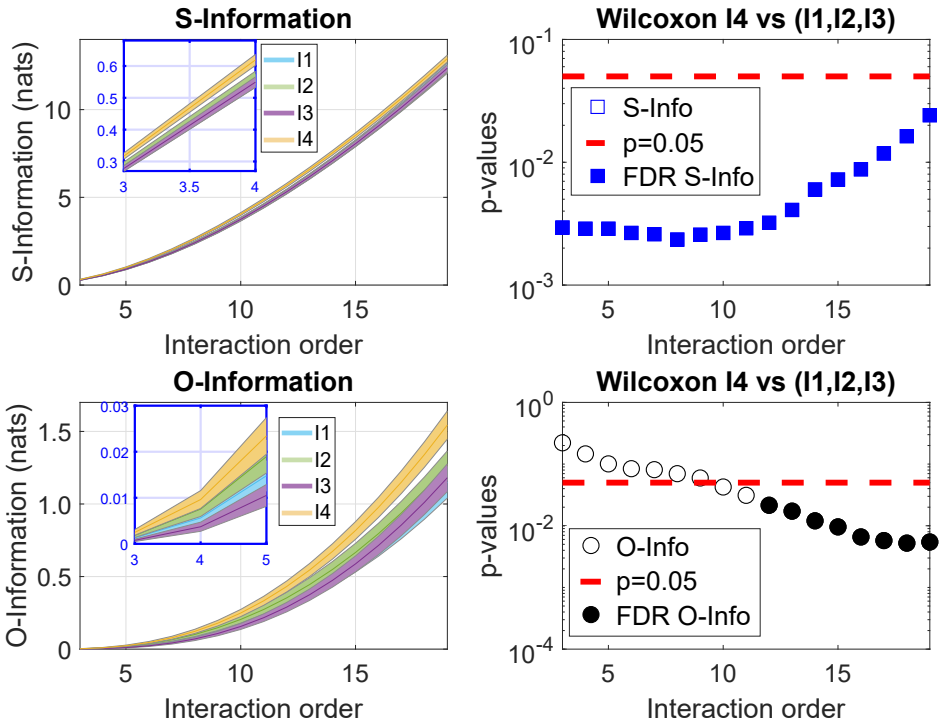

Figure 3.2: **High-order interdependencies in the aging brain**. Average O-information and S-information average over all modules $m = \{1, \ldots, 20\}$ from equations 5 and 6 for each subject, grouped as I1, I2, I3, I4. Both S-information (top panel) and O-information (bottom panel) differentiated the higher order interdependencies in the old brains (I4) relative to the younger ones (I1, I2 and I3). This is evident in the right column, where the statistical significance is represented either for a uncorrected p-value of 0.05 (red dashed line) or corrected by the FDR (represented by blue-filled squares for the S-information and by black-filled circles for the O-information). The interaction order is shown on the x-axis in all the plots.

3.2.2 A significant increase in redundancy in older participants

We split the interactions according to the sign of the O-information, adding the positive ones as a measure of redundancy, and negative ones as synergy. Our results show different patterns of redundancy and synergy as the interaction order increases (see Figure 3.3). While the synergy exhibits an inverted-U (concave) shape, redundancy monotonically increases with the interaction order. Importantly, the redundancy values are much larger than the synergistic ones. Moreover, the redundancy of I4 shows significant differences from the group formed by (I1, I2, I3) for all interaction orders. In the case

of synergy, while at some interaction orders the group I4 exhibits significant differences from the rest of the population, these differences do not survive the multiple comparison correction.

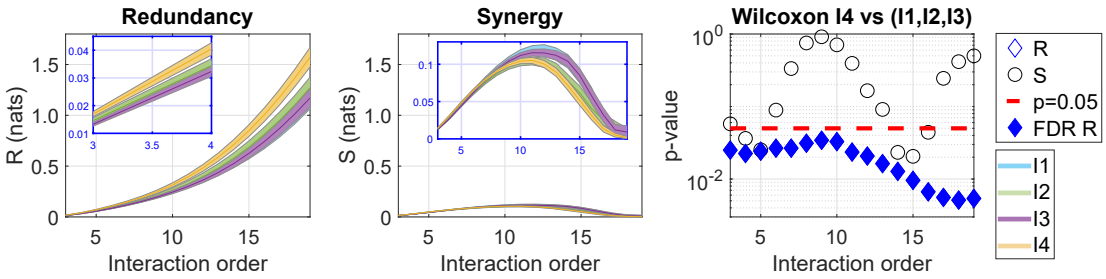

Figure 3.3: **A significant increase in redundancy in older participants across all interaction orders**. The average redundancy and synergy were obtained over modules $m = \{1, \ldots, 20\}$ through the equations (2.10) and (2.11) for each subject grouped into I1, I2, I3, I4. Note that when increasing the interaction order, and independent of age, both redundancy and synergy curves have a completely different pattern (one increasing linearly and the other following a bell-shaped curve). The right panel shows that the group differences in redundancy (represented by diamonds) in older participants (I4) were significantly different from those of the other groups combined (I1, I2, I3) for all interaction orders. Regarding synergy (represented by circles), none of the values survived a correction for multiple comparisons at any of the interaction orders. Both the diamonds and circles are filled when the value of redundancy or synergy survived correction for multiple comparisons.

3.2.3 Redundancy and synergy across the distinct brain areas

We quantified the redundancy across brain modules by taking into account all the redundant interactions in which a given module participate, Figure 3.4 shows that modules 1-3, 5, 13-15, 18-20 exhibit significant differences for all interaction orders, while the others only exhibit significant differences for large orders. This suggests the existence of a *redundancy core*, which was confirmed by later analyses. In contrast, the pattern of synergy across brain areas is highly heterogeneous, with only modules 15, 17, 18 and 19 showing significant differences.

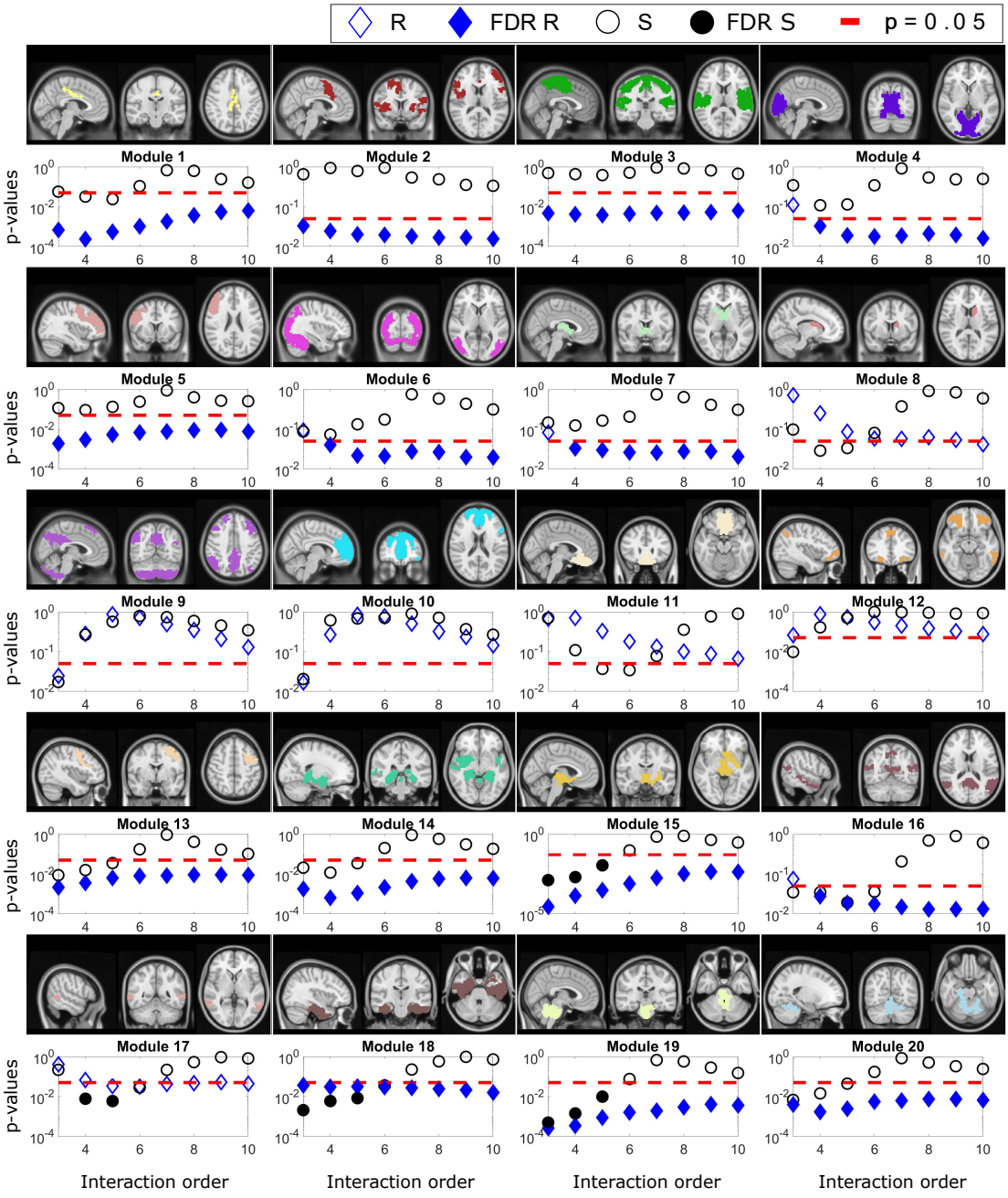

Figure 3.4: **Redundancy and Synergy across brain areas in the aging brain**. Differences between I4 and the I1, I2, I3 groups across the different brain modules, each one anatomically represented by three representative views from left to right, sagittal, coronal and axial. As in Figure 3, group differences in redundancy (blue diamonds) and synergy (black circles) are represented as a function of the interaction order. When the group differences survived FDR correction, both the diamonds and circles are filled. In relation to redundancy, there are two "classes" of modules, those where redundancy was significantly different for any order (such as modules 1-3, 5, 13-15 and 18-20) and the remaining modules for which this did not happen. Synergy generally does not differ widely between group I4 and the rest of the population across different brain areas. Modules 15, 17, 18, and 19 showed a few interaction orders with values surviving multiple comparisons.

3.2.4 Identification of the redundant and synergistic cores

To confirm the existence of a redundancy core, we studied the extreme values of the O-information for various interaction orders. Figure 3.5 shows how modules 2, 5 and 13 participate in the most redundancy-dominated n-plets for all orders, suggesting that they might be the basis of such a core. While a complete anatomical description of these modules is available in Ref. [70, 71], it is important to emphasize that these three modules have in common the middle frontal gyrus (MFG) and precentral gyrus (PG), two important structures that have a very differentiated function. More specifically, while MFG is part of the prefrontal cortex which mediates executive control and working memory, PG is part of the primary motor cortex, and the two structures are well-known to be affected by aging [4, 72, 73, 74].

It is important to emphasise that although the redundant role found in this study for the interaction between MFG and PG was obtained from participants being at rest, potentially it reflects the fact that older participants typically compensate motor behavioral deficits by recruiting additional activation of the prefrontal cortex in synchronism with their associated motor areas, while younger participants only activated motor areas to perform the same tasks [75, 76, 77]. Similarly, it has also been shown that older participants, but not young, recruit the prefrontal cortex while performing purely movement tasks such as the inhibitory motor control, thus relying on more cognitive support for the performance of a motor task that younger participants produce in a more automatic manner, i.e., cognitive penetration into action [78].

Interestingly, the core existing in younger participants (I1, I2 , I3) seems to be broader than the one in the older population, including modules 9, 10 and 16. The brain structures supporting these modules are composed of the middle and superior frontal gyri, posterior cingulate cortex and the precuneus, all part of the default mode network (DMN), which is an important network of the human brain (see [79, 80] and references therein). Despite the fact that other studies have found a lesser participation of the precuneus into the DMN [81], our data confirmed its participation in agreement with other studies [79, 82].

When comparing these results to the ones in Ref. [58], in which a redundant role of the DMN was shown for $n = 3$ across the lifespan, it could happen that for high orders of interaction such a role might break down in older participants, indicating network re-adaptation or anticipation to damage, as it occurs at the onset of other pathologies such as in the early stage of Alzheimer's disease [83], after a concussion [84] or following a multiorgan failure [85].

When looking at modules that participate in synergistic arrangements, i.e. at the n-plets with smaller values of O-information, we found that modules that belong to the redundant core tend not to be involved in very synergistic arrangements, with the exception of modules 9 and 16, which are are present in all groups of ages. These

two modules have in common the posterior cingulate and precuneus that, as explained above, are part of the DMN. Based on these results, we might hypothesize a dual redundant-synergistic role of the DMN, that, in older participants, it seems that the redundant contribution gets impaired.

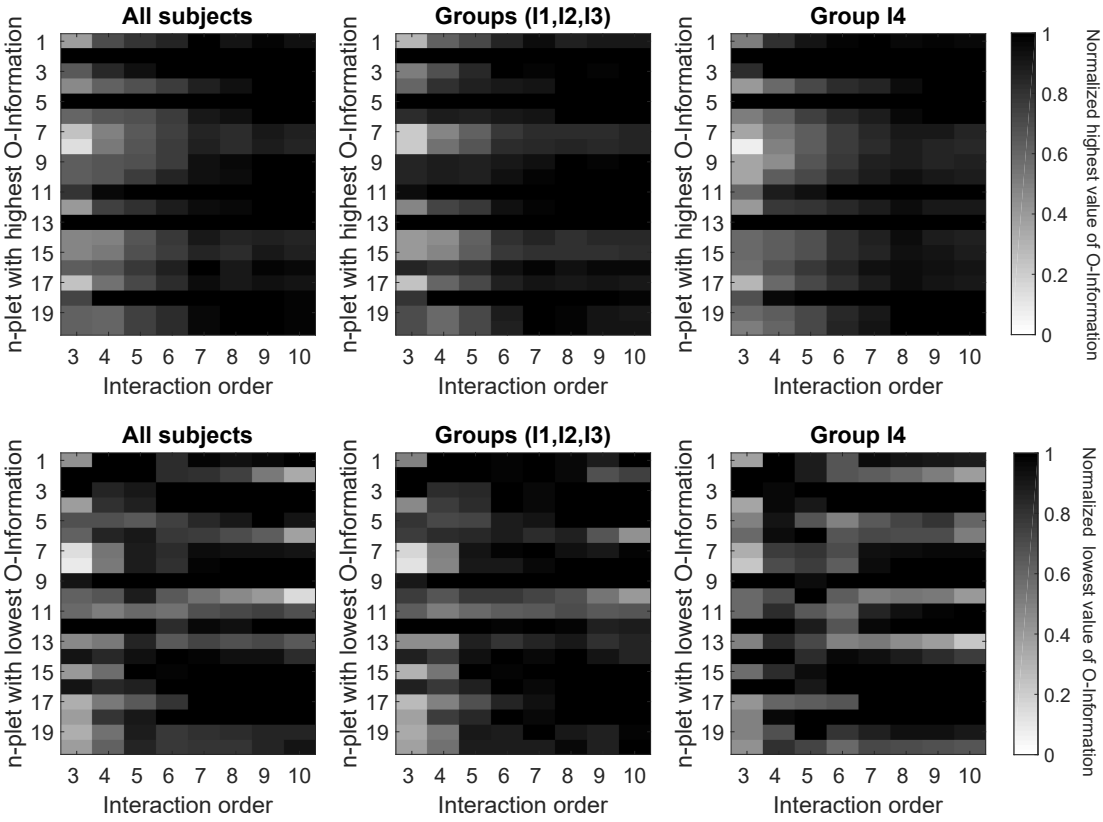

Figure 3.5: **Identification of the redundant and synergistic cores for the different interaction orders**. **Top row:** As a function of the interaction order$n$, we rank the averaged O-information values of all the n-plets per group of participants, as detailed in the Methods and illustrated in Figure 1 panel D. We plotted the highest O-information value in which each module participates for each interaction order, normalized to the n-plet with the highest O-information averaged in different groups of participants. For each interaction order the n-plet with the highest values of O-information are in black. The highest O-information values measure redundancy. **Bottom row:** As above but plotting the lowest values of O-information. Because all were negative, they corresponded to synergy. The two rows show similar plots for three different situations: all subjects (left); pooling I1, I2, and I3 together (middle); and for the older group, I4 (right).

3.3 Discussion

The present study assesses the high-order redundant and synergistic interactions among brain regions of participants of various ages. Overall, an important increase in redundant interdependencies in the older population was found for all interaction orders. Additionally, a redundant core of brain modules was observed, which decreased in size with age. Together, these two findings suggest a change in the balance of differentiation and integration towards more synchronized arrangements.

It is important to emphasise that our analysis goes beyond traditional brain-network approaches that focus on pairwise interactions, considering high-order interactions that can assess redundant and synergistic effects. In doing so, we follow the seminal ideas introduced by Tononi, Sporns, and Edelman [26], which posit that high brain functions might depend on the *co-existence of integration and segregation*. Indeed, while the latter enables brain areas to perform specialized tasks independently of each other, the former serves to bind together brain areas towards an integrated whole for the purpose of goal-directed task performance. A key insight put forward in Ref. [26] is that segregation and integration can coexist, and that this coexistence is measurable by assessing the high-order interactions of neural elements via approaches such as the one used in this study. In the context of aging, it has been shown that the balanced segregation-integration might break down as the inter-network connectivity increases in older people (reducing segregation). However, this increment does not correspond to a better performance, therefore indicating that the reduced segregation is related to neuronal disfunction, possibly due to the reduced inhibitory function found in older adults [45].

It is worth noticing that our results related to increased redundancy in aging cannot be cast in terms of pairwise interactions. Redundancy does not only implies that the implied areas share information, but that they share *the same* information. Please note that no (pairwise) network approach could discriminate this fact. Therefore, having more redundancy in the brain does not imply mere higher connectivity: it says that the same information is present in more than two places at the same time (the number depending the redundancy order), which in turn suggest a lost of specificity and a potential sub-optimal utilisation of resources.

3.4 Limitations and future work

The current study is based on the following methodological assumptions. First, the accurate quantification of redundancy in large-scale brain networks remains an open problem [86], but by using the Ω-measures of synergy-redundancy balance, we have proposed different metrics as proxy estimators for synergy and redundancy. Second, different brain parcellations can be used to explore high-order functional interactions in the brain, however, a finer spatial resolution compromises the calculation of all of the

n-plets to assess the O-information as the combinatorics becomes very large. Finally, the fact that the values of the O-information themselves suggest a predominance of redundancy might be heavily influenced by the nature of fMRI data, and other results might be seen from other kinds of measurements (e.g. EEG or MEG). What is relevant is the increase of O-information, which is clear evidence pointing towards a change of differentiation-integration balance towards more redundant arrangements.

3.5 Materials and Methods

Participants

A cohort of $N = 161$ healthy volunteers with an age ranging from 10 to 80 years (mean age 44.35 years, SD 22.14 years) were recruited in the vicinity of Leuven and Hasselt (Belgium) from the general population by advertisements on websites, announcements at meetings and provision of flyers at visits of organizations, and public gatherings. All subjects were informed before study participation and signed the informed consent. For minors, written informed consent was provided by their legal representative. The study was approved by the local Medical Ethics Committee of KU Leuven (study number: S60428) in accordance with the Declaration of Helsinki and its amendments (World-Medical-Association 1964, 2008).
None of the participants had a history of ophthalmological, neurological, psychiatric, or cardio-vascular diseases potentially influencing imaging measures. We grouped the participants into four age groups Ii for $i \in \{1, \ldots, 4\}$: I1 consists of $N_1 = 30$ subjects aged 10-20 years old; I2, $N_2 = 46$ subjects 20-40 years old; I3, $N_3 = 29$ subjects 40-60 years old; and I4 $N_4 = 59$ subjects 60-80 years.

3.5.1 Image acquisition and preprocessing

Image acquisition was performed on a MRI Siemens 3T MAGNETOM Trio MRI scanner with a 12-channel matrix head coil. The anatomical images were acquired with a 3D magnetization prepared rapid acquisition gradient echo (MPRAGE) and the following parameters: repetition time (TR) = 2,300 ms,echo time (TE) = 2.98 ms, voxel size = $1 \times 1 \times 1.1$ mm^3, slice thickness = 1.1 mm, field of view (FOV) = 256×240 mm^2, 160 contiguous sagittal slices covering the entire brain and brainstem. The anatomical images were then used for preprocessing of the functional data, here acquired with a gradient echo-planar imaging sequence over a 10 min session using the following parameters: 200 whole-brain volumes with TR/TE = 3000/30 ms, flip angle = 90, inter-slice gap = 0.28 mm, voxel size = $2.5 \times 3 \times 2.5$ mm^3, 80×80 matrix, slice thickness = 2.8 mm, 50 oblique axial slices, interleaved in descending order.
Functional imaging preprocessing was performed following a similar procedure to that in Ref. [58]. The preprocessing pipeline included slice-time correction, head motion arti-

facts removal, intensity normalization, regressing out of the average cerebrospinal fluid, average white matter and average global signal, bandpass filtering between 0.01 and 0.08 Hz, spatial normalization to a template of voxel size of $3 \times 3 \times 3$ mm^3, spatial smoothing, and scrubbing. This resulted in a total of 2514 time series of fMRI BOLD signal for each participant, corresponding to the functional partition used in Ref. [70]. Moreover, because for the calculation of high-order interactions at order n we have to deal with $n-$plets of region combinations (for details see the following subsections), we reduced complexity grouping the original 2514 regions into 20 final brain atlas regions, simply by averaging the time series of all regions within a given atlas region. For this stage, we made use of the Brain Hierarchical Atlas [70], that has been previously used [87, 88, 89]. The partition of 20 regions is the one that maximized the cross-modularity, a metric that accounts for the triple optimization of the functional modularity, the structural modularity and the similarity between structural and functional regions (for details see Ref. [70]).

To obtain the structural connectivity matrices, we acquired diffusion weighted single shot spin-echo echo-planar imaging (DTI SE-EPI) images with the following parameters: TR = 8,000 ms, TE = 91 ms, voxel size = $2.2 \times 2.2 \times 2.2$ mm^3, slice thickness = 2.2 mm, FOV = 212×212 mm^2, for each image, 60 contiguous sagittal slices were acquired covering the entire brain and brainstem. A total number of 64 volumes were acquired corresponding to different gradient directions with b=1000 s/mm^2. One extra 3D diffusion image was acquired for b = 0 s/mm^2, needed for the diffusion imaging preprocessing. Although full details are given in Ref. [90], the pipeline consisted in eddy current correction, motion correction, tensor estimation per voxel, fiber assignment, and functional partition projection to the individual diffusion space. This resulted in SC matrices of dimension 2514×2514, one per participant, and each matrix entry corresponding with the number of white matter streamlines connecting that given region pair. Finally, we reduced complexity of these matrices by grouping the 2514×2514 matrix into 20×20 using the BHA, and averaging the BOLD signals of all regions within a given atlas region. The BOLD signals and connectomes used in chapter 3 and 4 are available at `https://github.com/brincolab/High-Order-interactions/tree/master/dataset`

3.5.2 Parcellation

We use the Brain Hierarchical Atlas (BHA), both functional and structural parcellation, exploiting their intrinsic hierarchical modular organization. The algorithm behind consists in a maximization of the quantity Cross-modularity. This measure is used to define anallitically the relying principles by a function whose arguments are the functional modularity, the structural modularity, and the similarity between the functional and structural modules. The Cross-modularity has been calculated for brain partitions of different sizes, from 1 (the entire brain is one big cluster) to 100 modules, and the

optimum is around 20 modules.
It has to be noted that, compared to other parcellations that focus into the cerebral cortex, the BHA encompasses the whole brain including brainstem, cerebellum, thalamus, striatum, amygdala, hippocampus, and cerebral cortex.

4

High-order interdependencies in a whole-brain model

4.1 Introduction and hypothesis

Despite these considerable advances in understanding how the anatomical and functional connectivity change along the lifespan, the relationship between changes in brain structure and function leading to age-related decline remains largely unknown [30, 31, 32, 24]. In the previous chapter of this thesis, using functional neuroimaging data, we have shown that complex patterns of interactions between brain areas change along the lifespan, exhibiting increased redundant interactions in the older population. However, which mechanisms might underlie these functional differences is still unclear. Here, we extended this work and hypothesized that the variations of functional patterns might be explained by the changes of the brain's anatomical networks, which are known to degenerate as we age.

To bridge this important gap, we sought to investigate how age-related changes in brain structure affect its function. We tackle this fundamental question via whole-brain computational modeling, which is an emerging powerful tool to investigate the neurobiological mechanisms that underlie macroscale neural phenomena [91, 92, 93]. Our approach is based on the Dynamic Mean Field (DMF) model, which simulates mesoscale neural dynamics using coupled stochastic differential equations incorporating realistic aspects of neurophysiology [94, 95, 96]. DMF modeling can be used for systematically perturbing connectome characteristics while assessing the resulting effects on macroscale brain dynamics and function, thus opening the way to provide mechanistic modeling interpretations to data obtained from lesion studies and aging [97, 98, 99]. Furthermore, the different DMF inputs and biophysical parameters can be systematically altered in ways that are beyond the capabilities of current experimental research, which makes whole-brain computational modeling a privileged tool to investigate the causal mechanisms that drive the brain's organization and function [100, 101, 92, 102].

4.2 Results

Our analyses are based on the DMF model, which uses structural and functional connectivity matrices, (respectively SC and FC), to simulate the activity of various brain regions wired with SC in presence of local excitatory and inhibitory neuronal populations. A biophysical haemodynamic model [103] is then used to transform the DMF model's firing rate dynamics into BOLD-like signals. The DMF is calibrated by optimising a free parameter, denoted by G, that allows the model to best approximate pairwise functional activity [92]. This procedure is illustrated in Figure 4.1, and details are provided in methods.

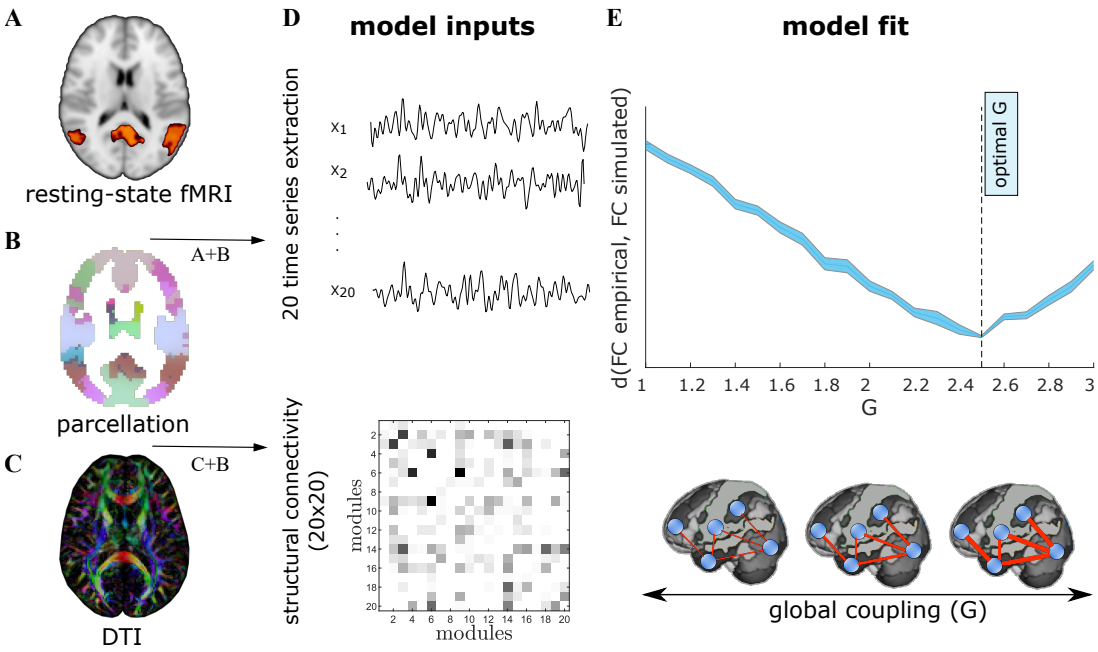

Figure 4.1: **Whole-brain Dynamic Mean Field Model**. The DMF model used has as inputs **A)** BOLD signals from fMRI data, **B)** a parcellation, in our case comprising 20 modules (or regions) and **C)** the connectome obtained from DTI. **D)** Applying the parcellation to the fMRI and DTI data we obtain 20 signals and a 20×20 matrix representing the connectome, respectively. **E)** BOLD-like signals are simulated using the connectome and different values of the coupling parameter G. For each G, we compare the simulated and empirical data using the Kolmogorov-Smirnov distance over the histograms obtained from the FC matrices, and select the optimal G as the value that minimizes this distance.

4.2.1 DMF model reproduces empirical differences in redundancy

To study the effect of aging on brain dynamics, we used functional data from different participants divided into four age groups, similar to previous work [104]: I1 ($N_1 = 28$ participants, age 10-20 years), I2 ($N_2 = 46$, 20-40 years), I3 ($N_3 = 29$, 40-60 years) and I4 ($N_4 = 58$, 60-80 years). One DMF model was built for each age group, using the average SC within each group (Figure 4.2A). Next, each model was calibrated separately, resulting in one G value per group (Figure 4.2B). For each model, we simulated the brain activity using different random seeds, and the high-order interdependencies were calculated from these simulated data. In particular, we calculated the O-information [53], which can be considered an extension of the neural complexity previously proposed in [26] under the light of Partial Information Decomposition [105]. In essence, the O-information captures the balance between redundancies and synergies in a set of interacting variables [55, 68] (for further details see Methods).

We computed the O-information for all the subsets of brain regions of size $3 \geq n \geq 20$, where n represents the interaction order. For each order, n-plets with positive and negative values of the O-information — called for simplicity 'redundancy' and 'synergy,' respectively — were calculated. Wilcoxon tests were performed to compare the average values of redundancy and synergy in the older participants (I4) with the values obtained from the groups of younger participants following previous work [104]. This is illustrated in Figure 4.2C. The DMF model reproduced the age differences in redundancy and synergy reported in [104]. Moreover, the differences in redundancy between I4 and the rest of groups (I1,I2,I3) are statistically significant at all orders after the multiple comparison correction of the false discovery rate. Interestingly, although the DMF model was fitted only using pairwise FC values, the simulated dynamics captures similar profiles of high-order statistics than our fMRI data.

4.2.2 A connectome-based model of brain aging

Motivated by the fact that the DMF model (connected with the average SC within each age group) reproduced the high-order interaction patterns of redundancy and synergy very precisely, we asked whether varying the SC of the young population was sufficient to reproduce the high-order functional aspects in the older participants. We then studied the relationship between the weights of SC from the youngest group I1 and the corresponding weights from the oldest group I4 through a parabolic fitting (for further details see Methods). This second-order polynomial fitting revealed a non-linear reduction of the anatomical weights throughout the brain, in agreement with previous work [39, 41, 24] (Figure 4.3A). Next, the fitted polynomial was used to simulate the effects of aging in each of the young participants belonging to I1, thus resulting in an "aged" version of their connectomes (Figure 4.3B). Each of these *synthetic* aged connectomes was used to run a set of simulations using the DMF with the optimal value

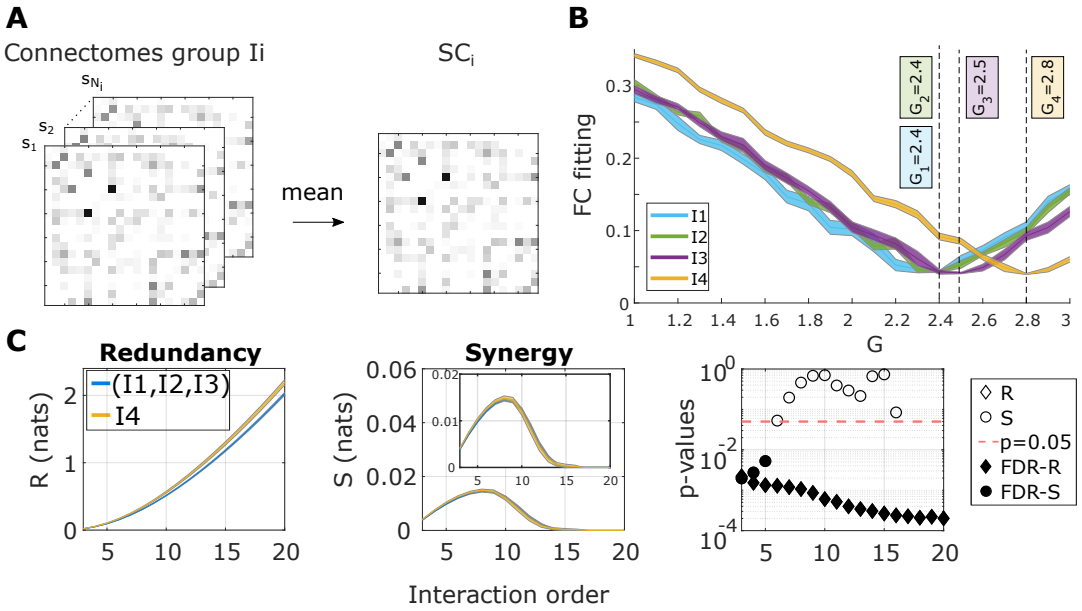

Figure 4.2: **The DMF model reproduces redundancy differences across age groups**. **A)** First, we compute the average structural connectivity matrix for each age group. **B)** Then, we find the optimal G value for each age group using the corresponding connectomes as input to the DMF. **C)** We simulate brain activity representative of each age group using the average connectome and the optimal value of G, compute O-information, and separate sets of modules into redundant (positive O-information values) and synergistic (negative O-information values). Here, redundancy and synergy are estimated as the average O-information of redundant and synergistic sets, respectively. The p-values of the Wilcoxon test to compare the I4 group versus the rest of the population in redundancy and synergy. When the value of redundancy (or synergy) survived the false discovery rate correction, the diamonds (or circles) are filled.

G_4. Finally, the high-order interactions of the simulated time-courses were calculated via separating the O-information into redundancy and synergy terms. Our results, illustrated in Figure 4.3C, showed that the synthetically simulated aged participants also reproduced the functional changes observed empirically, exhibiting significant (FDR-corrected) increased redundancy at all orders, with statistic values ranging from RS = 14462 ($p_{FDR} < 0.001$) to RS = 14264 ($p_{FDR} < 0.001$). Moreover, and to ensure that the good performance was not the result of simply taking G_4 into the DMF model of the younger group, the same analysis was repeated using the linear (rather than quadratic) model of connectome degeneration (Fig. S1). The linear aging model did not reproduce the redundancy differences observed between age groups, as they were not significant in none of the interaction orders studied. These results confirm that nonlinear heterogeneity in age-related connectome degeneration is crucial in explaining the observed changes in higher-order functional statistics. In the next section we delve into the topological structure of these anatomical changes.

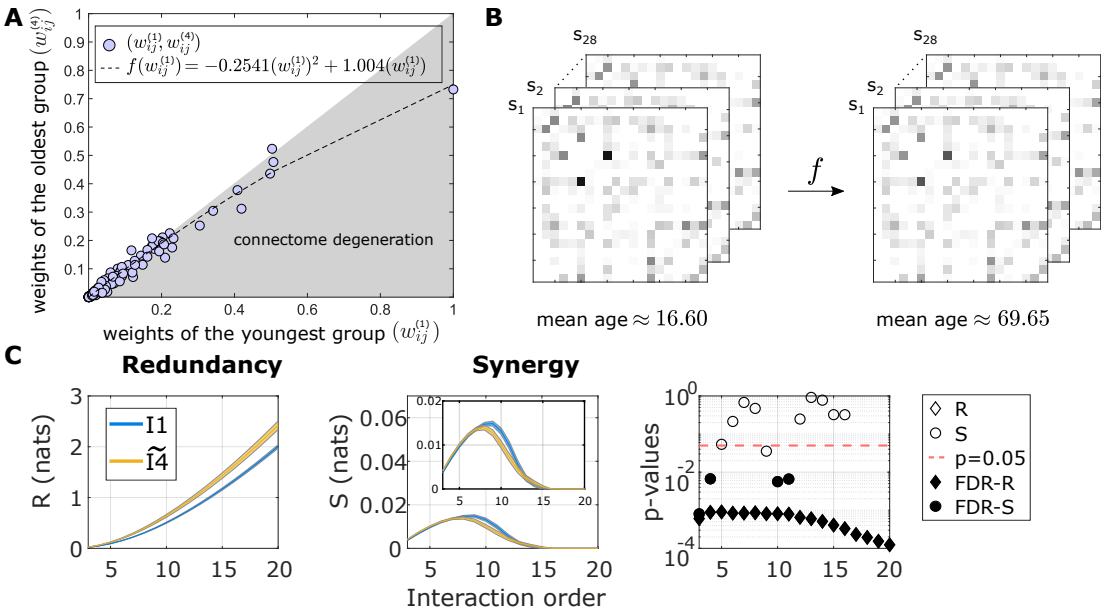

Figure 4.3: **Aging model based on the connectome**: **A)** A polynomial fit of second degree is made to link the weights of the average connectome of the group I1 denoted $w_{ij}^{(1)}$ and the weights of the average connectome of participants of the group I4 denoted $w_{ij}^{(4)}$, preserving the position/topology of the connectome. **B)** first panel twenty-eight empirical young connectomes. Second panel corresponds to applying the polynomial fit of panel A) to each young connectome obtaining surrogate older connectomes. **C)** We simulate the DMF model of the surrogate oldest connectomes and the optimal value G_4. The O-information is analyzed and separated into redundancy and synergy (first and second panel). The third panel corresponds to the p-values of the Wilcoxon test to compare the surrogate I4 group ($\tilde{I4}$) versus the youngest group (I1) in redundancy and synergy. When the value of redundancy or synergy survived correction, both the diamonds and circles are filled.

To ensure that the good performance was not the result of simply taking G_4 in the DMF modeling of the youngest group, the same analysis was repeated using a linear (instead of quadratic) model of connectome degreneration. The linear aging model did not reproduce the observed redundancy variations between age groups, confirming that the non-linear heterogeneity in the age-related connectome degeneration is crucial to explain the observed changes in the high-order functional statistics. In the following section we dive deeper into the topological structure of these anatomical changes.

4.2.3 Inhomogeneous neurodegeneration rates reveal two major communities of age-related brain links

We have shown that our model of connectome degeneration based on a second degree polynomial reproduces the statistically significant differences in the redundancy between the oldest group and the rest in all interaction orders studied. Interestingly, non-linearity implies that not all the links in the connectome age in the same way.

To further investigate the effects of age across brain regions, we evaluated the association between SC weights and age in all participants in our cohort (N=161), calculating the Spearman's correlation r between the participant age and each link of the SC matrix. This is illustrated in Fig. 4.4A. To study the aging process at the aggregate or module level (beyond the relationship between weight with age at the single link level), using the absolute correlation values as links of a new matrix (left panel in Fig. 4.4B), we applied the Louvain's community detection method obtaining three distinct link communities (note that community detection was applied to the matrix of r values before the multiple comparison correction). In addition, the different links within the three communities that survived the Bonferroni correction have values of r ranging from -0.25 to -0.5, thus showing a reduction in SC values with age. Regarding the stability of the Louvain's method to maximize network modularity, we varied the resolution parameter γ (see Methods) and obtained the same three communities for values of γ ranging between 0.9 and 1.2, which shows the stability of our network partition in the three communities found.

The first community only had two significant links (right panel in Fig. 4.4B), and for this reason we considered it as a less relevant community. The second community was dominated by interactions involving brain atlas regions 15 and 18 (Fig. S2), as these two nodes had the highest values of node strength (here, calculated over the graph of r absolute values). These regions encompass several subcortical structures, such as the striatum, thalamus, brain stem, amygdala and the hippocampus (for a complete description of all regions in the atlas, see Refs. [70, 71]). In contrast, the third community, with higher strength values for regions 6,9 and 20 of the atlas, was dominated by a common structure present in these three regions, which is the cerebellum. Therefore, the two communities exhibited age-induced reduction in within-community correlations, but in one, the degeneration was centered around striatum and hippocampal connectivity, and in the other around the cerebellum.

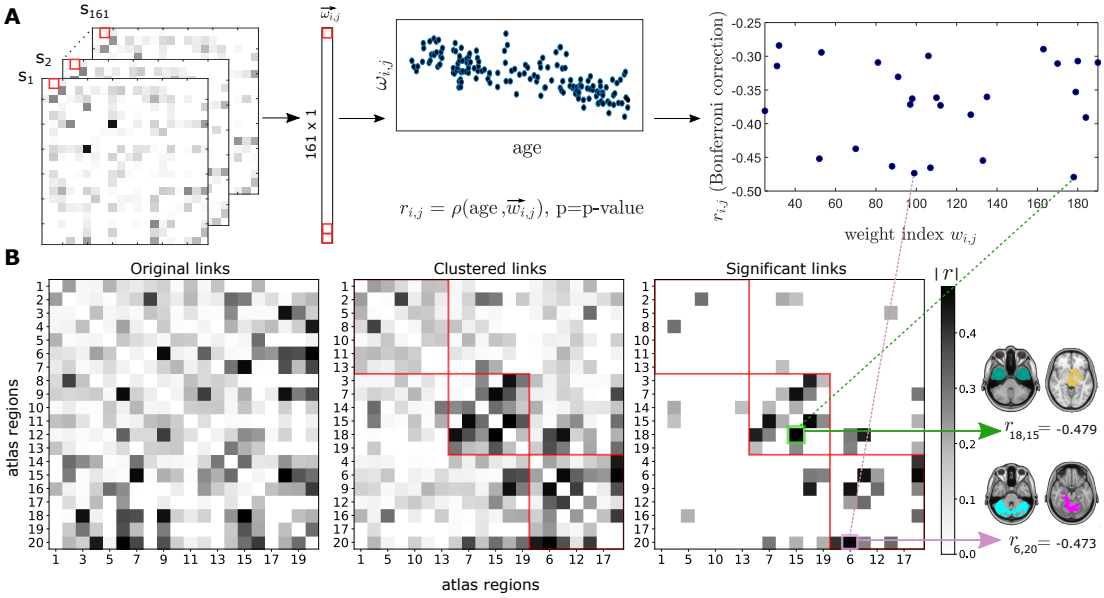

Figure 4.4: **Heterogeneity of the connectome degeneration**: **A:** The non-parametric Spearman's rank-correlation r between age and individual weights w_{ij} of the SC matrix was calculated across all the different participants (N=161). A correction for multiple comparisons was also applied. The final number of weights which survived to multiple comparisons is represented in the right panel, with values ranging from -0.25 to -0.50. **B:** We built a new connectivity matrix using as links the values of r obtained for each weight (left panel). After applying the Louvain's method of community detection to this matrix, three major communities were found (center), and the communities had significant values of links (right). As an illustration, we showed one arbitrary link within each of these communities (colored in green and pink).

4.3 Discussion

In this thesis we used a combination of functional and diffusion MRI data together with DMF whole-brain modeling to investigate the mechanisms underlying age-variations in the structure of high-order functional interactions. The DMF model successfully reproduced the increased redundancy-dominated interdependencies of BOLD activity across brain areas in the older participants, and across all interaction orders, in full agreement with recent observations Ref. [104]. Furthermore, we provided evidence that these high-order functional changes are driven by localized non-lineal processes of neurodegeneration in the connectome. Leveraging this finding, we proposed a non-linear connectome-based degeneration model of aging, which can be applied to young connectomes to simulate age-induced changes in functional brain patterns.

Whole-brain models of neuronal activity have significantly increased our understanding of how functional brain states emerge from their underlying structural substrate, and have provided new mechanistic insights into how brain function is affected when other

factors are altered such as neuromodulation [92, 106, 107], connectome disruption [102, 108], or external stimuli [109, 110]. Adding to these findings, the present results provide a causal link between a localized connectome-based degeneration model of aging and age-variations of high-order functional interdependencies. These results establish a first step towards explaining how the reconfiguration of brain activity along the lifespan intertwines with changes in the underlying neuroanatomy.

Our results revealed two communities with differentiated age-induced deteriorated connectivity, one focused on the striatum and hippocampus, and the other on the cerebellum. In relation to striatal connectivity, previous studies showed that the fronto-striato-thalamic circuit was the most dominant for age prediction in healthy participants [90]. Moreover, age-related deterioration of striatal connectivity has also been associated with reduced performance in rest [46] and action selection tasks [111], inhibitory control [112], and executive function [113]. In relation to hippocampus, a gold-standard structure affecting memory-impaired degenerative diseases, is also affected in normal aging [114], with implications in spatial and episodic memories processing [115]. In relation to cerebellar connectivity, both sensorimotor and cognitive task performance in the older population has been shown to be associated with cerebellar engagement with the default mode network and striatal pathways [116]. The connectivity between cerebellum and striatum was also shown to be affected by age and exhibited relations with motor and cognitive performance [117]. Therefore, our results provide further support for the important behavioral implications that age-disconnection has on these circuits.

4.4 Limitations and future work

This work makes use of a brain parcellation of only 20 regions from the brain hierarchical atlas (BHA) [70]. It has to be noted that, compared to other parcellations that focus into the cerebral cortex, the BHA encompasses the whole brain including brainstem, cerebellum, thalamus, striatum, amygdala, hippocampus, and cerebral cortex. While this parcellation was shown to maximize the cross modularity index between the functional and structural data, future work may also consider other brain parcellations to elucidate the robustness of our results by studying if age related changes in SC can also explain the differences high-order functional interactions in whole brain models. Analogously, some variations in the MRI preprocessing pipeline could also affects our results [118], as previous works have shown that affect pairwise FC studies [119].

In this article, we have fit the DMF model based on pairwise functional connectivity, reproducing the findings observed in Ref. [104] that the brain dynamics of older participants were significantly more redundant than the rest of the participants at all interaction orders studied. Furthermore, the use of quadratic connectome degeneration dynamics in addition to the pairwise-fitted FC model was sufficient to reproduce these high-order group differences, as pairwise-fitting with linear aging dynamics did not re-

produce these results. However, other findings were also reported in Ref. [104], such as the existence of a redundant core specific to the older subject group that cannot be reproduced by fitting only pairwise functional connectivity (results not shown). Several causes could explain this; for instance, we have an average connectome per age group, which provides a global parameter G per group used in all our simulations. It is possible that fitting a different model for each participant could introduce more heterogeneity, which could perhaps help improve the precise match between the actual data results and our modeling approach. A radically different alternative could have been to build models by fitting the structure of higher-order functional interactions beyond pairs, which is of great interest to explore in future work, likely providing a better fit to the data and perhaps also allowing the model to makes novel predictions, thus opening up new and exciting possibilities.

Finally, our analyses assessing high-order functional interactions are based on some specific metrics such as mean values of O-information at each interaction order. Future studies may consider different algebraic or topological properties of the full O-information hypergraph [120, 121, 122, 123, 124, 125], which may provide complementary insights. It is also worth noting that the reported values of the O-information are not indicative of 'pure' synergy or redundancy, but correspond to the balance between them. The O-information was chosen because it is a convenient measure to assess high-order effects up to relatively high orders. However, the O-information is a whole-minus-sum type of measure, and hence its analysis does not fully discriminate e.g. net increases in redundancy from decreases in synergy. Future studies could perform more detailed analyses by employing partial information decomposition (PID) measures [126, 127, 86, 128, 129, 130, 131, 132].

4.5 Materials and Methods

4.5.1 Neuroimaging

Please refer to the Materials and Methods section of the previous chapter.

4.5.2 Whole-Brain Dynamic Mean Field Model

To simulate neuronal activity we used a Dynamic Mean Field Model (DMF) [95, 92]. A brain region is modelled by a node n composed of inhibitory (I) and excitatory (E) pools of neurons interconnected, where the inhibitory currents $I^{(\mathrm{I})}$ are mediated by GABA-A receptors, the excitatory synaptic currents $I^{(E)}$ are mediated by NMDA receptors. The connectivity between two different nodes n, p is given by the $C_{n,p}$ value of the connectome (structural connectivity matrix C), the nodes are coupled by excitatory currents.

The DMF consists of a coupled system of differential equations:

$$
\begin{aligned}
I_n^{(\mathrm{E})} &= W_{\mathrm{E}} I_0 + w_+ J_{\mathrm{NMDA}} S_n^{(\mathrm{E})} + G J_{\mathrm{NMDA}} \sum_{p=1}^{N} C_{np} S_p^{(\mathrm{E})} - J_n S_n^{(\mathrm{I})} \ , \\
I_n^{(\mathrm{I})} &= W_{\mathrm{I}} I_0 + J_{\mathrm{NMDA}} S_n^{(\mathrm{E})} - S_n^{(\mathrm{I})} \ , \\
r_n^{(\mathrm{E})} &= F\left(I_n^{(\mathrm{E})}\right) = \frac{g_{\mathrm{E}}\left(I_n^{(\mathrm{E})} - I_{\mathrm{thr}}^{(\mathrm{E})}\right)}{1 - \exp\left\{-d_{\mathrm{E}}\, g_{\mathrm{E}}\left(I_n^{(\mathrm{E})} - I_{\mathrm{thr}}^{(\mathrm{E})}\right)\right\}} \ , \\
r_n^{(\mathrm{I})} &= F\left(I_n^{(\mathrm{I})}\right) = \frac{g_{\mathrm{I}}\left(I_n^{(\mathrm{I})} - I_{\mathrm{thr}}^{(\mathrm{I})}\right)}{1 - \exp\left\{-d_{\mathrm{I}}\, g_{\mathrm{I}}\left(I_n^{(\mathrm{I})} - I_{\mathrm{thr}}^{(\mathrm{I})}\right)\right\}} \ , \\
\frac{dS_n^{(\mathrm{E})}(t)}{dt} &= -\frac{S_n^{(\mathrm{E})}}{\tau_{\mathrm{NMDA}}} + \left(1 - S_n^{(\mathrm{E})}\right)\gamma r_n^{(\mathrm{E})} + \sigma v_n(t) \\
\frac{dS_n^{(\mathrm{I})}(t)}{dt} &= -\frac{S_n^{(\mathrm{I})}}{\tau_{\mathrm{GABA}}} + r_n^{(\mathrm{I})} + \sigma v_n(t)
\end{aligned}
$$

where the synaptic gating variable of excitatory pools is denoted by $S_n^{(\mathrm{E})}$ and the synaptic gating variable of inhibitory neurons population by $S_n^{(\mathrm{I})}$. The excitatory and inhibitory firing rates are denoted by $r_n^{(\mathrm{E})}$ and $r_n^{(\mathrm{I})}$ respectively. The feedback inhibitory control weight, J_n, was adjusted for each node n such that the firing rate of the excitatory pools $r_n^{(\mathrm{E})}$ remains clamped at 3Hz, using the linear fitting proposed by Herzog and colleagues [102]. The parameters used here are are listed in Table 4.1

Hemodynamic model

We used the excitatory firing rates $r_n^{(\mathrm{E})}$ to simulate BOLD-like signals from a generalized hemodynamic model [133]. An increment in the firing rate $r_n^{(\mathrm{E})}$ triggers a vasodilatory response s_n, producing blood inflow f_n, changes in the blood volume v_n and deoxyhemoglobin content q_n. The corresponding system of differential equations is

$$
\begin{aligned}
\frac{ds_n}{dt} &= 0.5 r_n^{(\mathrm{E})} + 3 - k s_n - \gamma\left(f_n - 1\right) \\
\frac{df_n}{dt} &= s_n \\
\tau \frac{dv_n}{dt} &= f_n - v_n^{\alpha^{-1}} \\
\tau \frac{dq_n}{dt} &= \frac{f_n (1-\rho)^{f_n^{-1}}}{\rho} - \frac{q_n v_n^{\alpha^{-1}}}{v_n}
\end{aligned}
\tag{4.1}
$$

where ρ is the resting oxygen extraction fraction, τ is a time constant and α represents the resistance of the veins. The BOLD-like signal of node n, denoted $B_n(t)$, is a nonlinear function of $q_n(t)$ (deoxyhemoglobin content) and $v_n(t)$ (blood volume):

$$
B_n = V_0\left[k_1\left(1 - q_n\right) + k_2\left(1 - q_n/v_n\right) + k_3\left(1 - v_n\right)\right] \tag{4.2}
$$

Table 4.1: Dynamic Mean Field (DMF) model parameters

Symbol	Parameter name	Value
I_0	External current	0.382 nA
W_{E}	Excitatory scaling factor for I_0	1
W_{I}	Inhibitory scaling factor for I_0	0.7
w_+	Local excitatory recurrence	1.4
J_{NMDA}	Excitatory synaptic coupling	0.15 nA
$I_{\mathrm{thr}}^{(\mathrm{E})}$	Threshold for $F(I_n^{(E)})$	0.403 nA
$I_{\mathrm{thr}}^{(\mathrm{I})}$	Threshold for $F(I_n^{(\mathrm{I})})$	0.288 nA
g_{E}	Gain factor of $F(I_n^{(\mathrm{E})})$	310 nC^{-1}
g_{I}	Gain factor of $F(I_n^{(\mathrm{I})})$	615 nC^{-1}
d_{E}	Shape of $F(I_n^{(\mathrm{E})})$ around $I_{\mathrm{thr}}^{(\mathrm{E})}$	0.16 s
d_{I}	Shape of $F(I_n^{(\mathrm{I})})$ around $I_{\mathrm{thr}}^{(\mathrm{I})}$	0.087 s
γ	Excitatory kinetic parameter	0.641
σ	Amplitude of uncorrelated Gaussian noise v_n	0.01 nA
τ_{NMDA}	Time constant of NMDA	100 ms
τ_{GABA}	Time constant of GABA	10 ms

where V_0 represent the fraction of venous blood (deoxygenated) in resting-state, and $k_1 = 2.77$, $k_2 = 0.2$, $k_3 = 0.5$ are kinetic constants [133].
The system of differential equations (4.1) was solved with the Euler method, using an integration step of 1 ms. The signals were band-pass filtered between 0.01 and 0.1 Hz with a 3rd order Bessel filter.

Simulation

We use the DMF implementation in Matlab freely available at `https://gitlab.com/concog/fastdmf`. The DMF equations are solved using the Euler scheme with integration step $dt = 0.0001s$ and 500 simulation time-points removing the first 20. The hemodynamic model is solved by the Euler method with an integration step $dt = 0.001s$ and subsampling each 3s. Finally, we obtain 160 time-points of BOLD signals corresponding to 8 minutes.

Model fitting

We run the DMF model using the average connectome SC_i consisting on the mean across connectomes belonging to the age group Ii. The DMF model has one free parameter G,

corresponding to the global coupling of neuronal populations. We fitted this parameter once per age group, where G_i denotes the optimal G value for the group Ii, $= \{1, 2, 3, 4\}$. To choose the simulations more alike to the empirical data, we compare them using the Kolmogorov–Smirnov distance between the functional connectivity matrix distributions built from the mutual information of the empirical and the simulated data. We swept the parameter G between 1 and 3 with steps of size 0.1. For each G value, we run 112 simulations using different random seeds. We obtained a convex curve where the x-axis represents the G values and the y-axis is the Kolmogorov–Smirnov distance. The minimum G value in the curve represents the optimal model.

4.5.3 Connectome aging model

We consider the data set $\left\{(w_{ij}^{(1)}, w_{ij}^{(4)})\right\}_{1\leq i<j\leq 20}$ as the edges in the upper triangular part of the average structural connectivity corresponding to the youngest population SC_1 and the average structural connectivity of the older population SC_4, respectively, for two different modules i, j. We propose a model for aging connectomes using a second-degree polynomial $f(w_{ij}^{(1)}) = a\big(w_{ij}^{(1)}\big)^2 + bw_{ij}^{(1)}$, where a and b are fitted from the empirical data. Then, we apply f on each edge of the twenty-eight empirical connectomes in the group I1 to create a surrogate elder connectome for each young connectome, which means $\tilde{w_{ij}}^{4,s} = f\big(w_{ij}^{1,s}\big)$ with $s = \{1, \ldots, 28\}$. Finally, we used the 28 surrogate connectomes and the parameter $G_4 = 2.8$ as inputs for the DMF. For each surrogate structural connectivity, we run four simulations and obtained in total 112 whole-brain simulations of the surrogate population.

Communities of age-related links

We first assessed the association for each individual connection and age. To do so, we calculated the non-parametric Spearman's rank-correlation between each entry of the SC matrix and age, using the different participants as observations (N=161). To find different communities of age-related brain links, we used the Louvain community detection algorithm available in the Brain Connectivity Toolbox [25] applied to the matrix of absolute values of the Spearman's r values. The optimal partition of the network corresponds to a subdivision of groups of nodes (or communities) that do not overlap and that maximize the modularity of the network, a metric that increases or decreases respectively when intra-community connectivity is high or intercommunity connectivity is low. To check the stability of the communities found by the Louvain method, we vary the resolution parameter γ (a hyperparameter that controls the trade-off between the actual number of edges in a community and the expected number of edges in the same community), and compute the partition integrity coefficient by evaluating the Spearman rank correlation between the two solutions for $\gamma = 1$ and the corresponding one for each of the different simulated values of γ. The network nodes

were the 20 brain regions of the Brain Hierarchical Atlas [70], and the links were the absolute value of the Spearman's correlation coefficients. After applying the community detection algorithm, we pruned the non-significant links using a Bonferroni correction.

5

High-order interactions applied to Frontotemporal Dementia

5.1 Introduction

The previous chapters have focused on describing high-order interdependencies in healthy brain aging and explaining how the age-related structural changes affect these high-order functional interactions using both data-driven and whole-brain computational modeling. This chapter analyzes and characterizes the changes in high-order interdependencies between a healthy population and patients with Frontotemporal Dementia.

Dementia affects around 55 million people worldwide, and Alzheimer's disease is the most frequent form, accounting for 60 to 70 percent of cases [134], but another highly prevalent form is Frontotemporal Dementia (FTD), primarily affecting the frontal and temporal lobe [135, 136, 137]. FTD encompasses a clinical spectrum that includes the behavioral variant FTD (bvFTD), semantic variant primary progressive aphasia (svPPA), and non-fluent variant primary progressive aphasia (nfvPPA) [138]. The bvFTD is characterized by changes in personality and/or a deterioration of cognitive features [139], whereas the progressive aphasia (PPA) is typically associate with a progressive disorder of language [140].

The bvFTD is the most common variant of FTD, and the best characterized. Many studies on rs-fMRI in bvFTD have focused on pairwise functional correlations. While it is true that some apparent contradictory findings have been found in the default mode network, showing mixed effects as hyper- and hypo-connectivity in the DMN [141, 142], thus emphasizing some of the heterogeneous aspects of this disease, a general finding is the hypo-connectivity in the salience network (another well-known resting-state network) [143]. However, up to date, there are no analyses of high-order interdependencies assessing redundancy and synergy in FTD. Therefore, we quantifie higher-order interdependencies for a brain parcellation with higher spatial resolution than in previous chapters, and where explicit calculations at higher orders than n=3 were not computationally feasible. We hypothesize that redundancy and synergy at order three might

be informational markers to describe the changes in brain activity produced by Frontotemporal Dementia.

5.2 Results

We analyzed resting state data publicly available from the NIFD database. The cohort is composed of 40 healthy control (HC) and 35 FTD subjects. The two groups are balanced in sex (p-val=0.20, ES=0.29), age (p-val=0.10, ES=0.37), and years of education (p-val=0.07, ES=0.41) (Table 1).

Variable	**HC**	**FTD**	**t-val**	**p**	**effect-size**
N	40	35			
Age, years	67.29 (4.34)	65.77 (3.67)	1.62	0.10	0.37
Females, %	23 (57%)	15 (43%)	1.60	0.20	0.29
Education years	17.10 (1.75)	16.14 (2.76)	1.81	0.07	0.41

Table 5.1: **Demographic variable of the HCs and FTD patients.**

We first compared T1-weighted anatomical images at the voxel level, performing voxel-based morphometry group comparison between HC and FTD. We found significantly less volume in FTD (also known as atrophy) in the striatum (accumbens, caudate, putamen), temporal pole (hippocampus, etorihinal, parahippocampal), amygdala and thalamus. To analyze the effect of Frontotemporal Dementia on brain dynamics, we proposed an analysis based on a redundancy and synergy count following the methodological scheme of Figure 5.1. First, we reduced the whole-brain neural dynamics of each subject into 86 representative time series. The 86 regions of interests (ROIs) contain 68 cortical areas from the Desikan-Killiany Atlas [144] and 18 subcortical regions. Then, for each subject, we computed the O-information for all the triplets without repetition present in the 86 ROIs (Figure 5.1 B). We next performed a surrogate strategy to assess the significance in the non-zero O-information values for each participant. In particular, a surrogate time series consisted in a lag-shifted time series realization of the original one using periodic boundary conditions. Next, for each triplet, we counted across participants in the groups of HC and FTD, the number of positive and negative O-information significant values, corresponding respectively to redundancy and synergy (Figure 5.1 C). Finally, we compared these numbers of redundant and synergistic counts between the groups using the Chi-squared test test (χ^2)(Figure 5.1 C) obtaining a p-value and a Chi-squared statistic (χ^2stat) per each triplet.

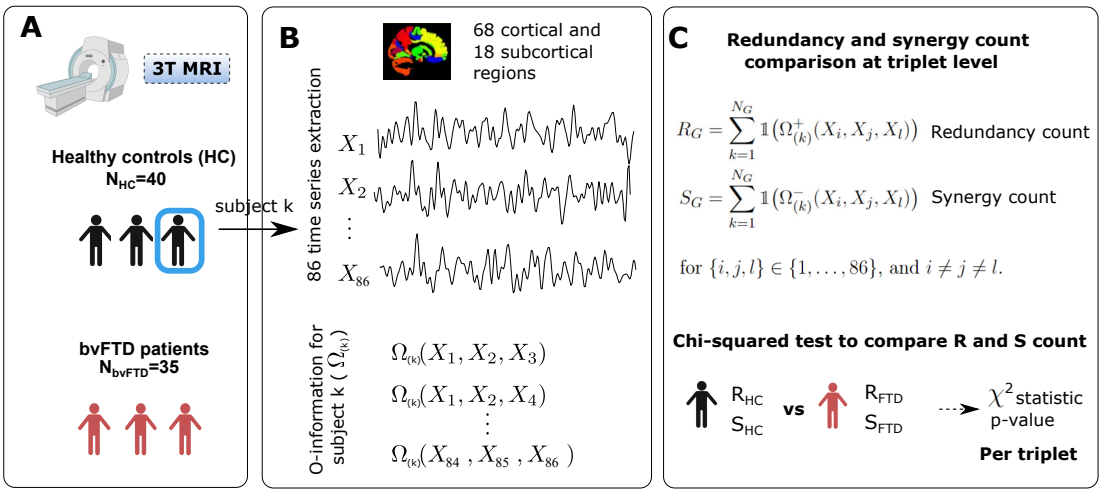

Figure 5.1: **Methodological scheme.** 75 subjects' fMRI data were extracted from the publicly available NIFD database and grouped into healthy controls (HC) and Frontotemporal Dementia (FTD). B. We grouped the time series into 86 ROI's, with 68 cortical regions from the Desikan-Killiany Atlas and 18 subcortical regions. Then, for each subject, we estimated the O-information at order three. C. For each triplet (groups of three ROIs), we count how many times the triplet was positive (redundancy count) or negative (synergy count) across subjects in each group. Finally, we compared the synergy and redundancy count between controls and patients using the Chi-squared test for each triplet.

5.2.1 Significant redundant and synergistic differences between HC and FTD after clustering correction

A total number of 102.340 Chi-squared tests were performed –coinciding with the number of triplets without repetition in the 86 ROIs– leading to a big multiple comparison problem. To overcome this issue, we followed a clustering method similar to the threshold-free cluster enhancement (TFCE) [145]. In particular, we first fixed a threshold τ and identified the triplets with χ^2stat value higher than τ (Figure 5.2A). Next, the survivor's triplets were grouped together if they shared at least one ROI in common. We next assigned a score to each cluster, corresponding to the sum of the χ^2stat triplet values within the same group (Figure 5.2A). Finally, we calculated a p-value for each cluster using surrogates of random permutations of the labels HC and FTD (y-axis, Figure 5.2B).

This strategy was repeated for different values of τ ($5 \leq \tau \leq 14$). The "best" value of τ, corresponding to the one with the lowest p value, occurred for $\tau = 10$, depicted in orange color in Figure 5.2B. For this value of τ, we found 54 statistically significant different triplets. Moreover, 72 of the total 86 ROIs participated in at least one triplet. Please note that in Figure 5.2A, we plotted a subset of the 102.340 triplets, and for this

reason, we showed only three of the 54 triplets belonging to the cluster.

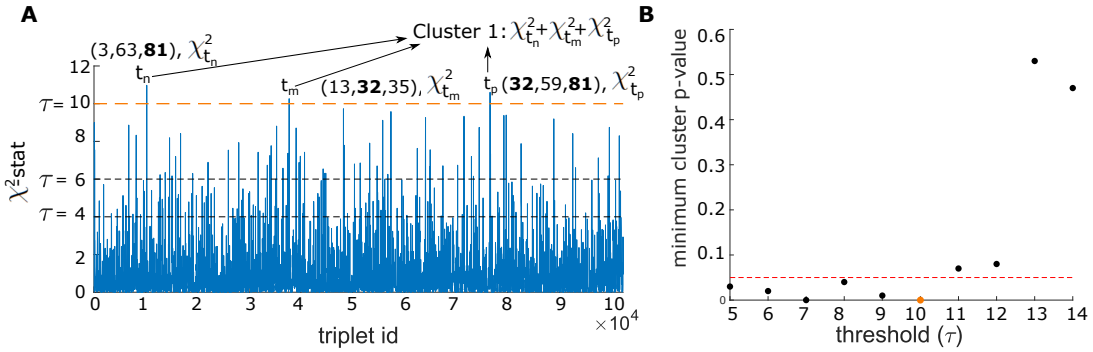

Figure 5.2: **Clustering correction method for HC vs. FTD.** A. A clustering method was performed for different thresholds τ. First, for each value τ we identified the triplets with statistic value higher than τ. Next, the survivor's triplets were grouped in the same cluster if they shared at least one region. For clarification purposes, the figure shows three triplets belonging to the same cluster. B. The clustering method depicted in A was performed for several thresholds (x-axis). A p-value (y- axis) was obtained for each cluster by comparing its size to clusters created from surrogate data.

5.2.2 Regions with unique redundant or synergistic participation

The cluster composed of 54 triplets with significant differences in redundancy and synergy between controls and patients contained two classes of triplets. The first one corresponded to those triplets where FTD was more redundant than HC (left circle in Figure5.3A) and the second one to those with HC more redundant than FTD (right circle in Figure5.3A). Please note that the second class is equivalent to the situation where FTD was more synergistic than HC. Indeed, as we compared only the subjects with significant non-zero O-information, redundancy and synergy act as complementary measures. For instance, if a triplet had 80% of redundant values, it had a 20% of synergy across a particular group (HC or FTD, Figure5.3A).

Then, we analyzed the ROIs belonging only to one of the two former classes to identify those ROIs with exclusive redundant participation, exclusive synergistic participation, or a combination of both, meaning that for some of the triplets those ROIs can have a redundant role, and in other triplets, a synergistic one. The ROIs participating in all significant triplets as redundant were the fusiform, posterior cingulate, and anterior cingulate (Figure5.3B, brain in red color). Similarly, the exclusively synergistic regions were the transverse temporal gyrus, also known as Heschl's gyri (Figure5.3B, brain in blue color). A third group of regions had a mixed participation, and their location included almost the entire frontal lobe (middle, inferior, and superior frontal), the inferior parietal, the isthmus of the cingulate gyrus, and the precentral cortex (Figure5.3B, brain in green color). Very importantly, the differences in high-order interdependences

were located in different regions of those altered at the morphological level, previously obtained by voxel-based morphometry.

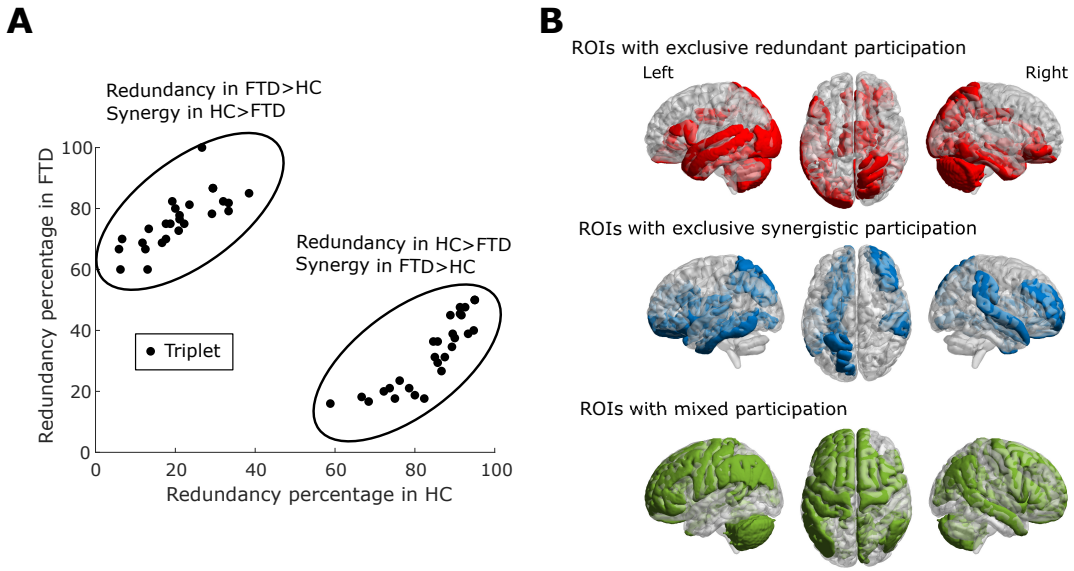

Figure 5.3: **Triplets visualization.**A. Percentage of patients within the FTD group that had a redundant interaction in a given triplet (y axis) as a function of the same percentage but in the HC group (x axis). Only the triplets with significant group differences in the redundancy/synergy ratio are depicted. B. Across all significant triplets, ROIs that had exclusive redundant participation (red), exclusive synergistic participation (blue), and mixed participation (some of the triplets in which ROI participated were redundant, and others were synergistic).

5.3 Discussion

Continuing with the previous chapters, we have focused on the characterization of HOIs and, in particular, on their differences between a group of HC and a group of patients with FTD. It is important to point out that, instead of averaging triplets within each BHA module as was done in previous chapters, in this chapter and as a novelty in the study of the high order interdependences, we chose to do the analysis at the level of individual triplets. This is important, as frontotemporal dementia is known to neurodegenerate some regions more than others and, in particular, pronounced atrophies were shown in frontal and temporal areas [135, 143, 136], striatum [146, 147], and thalamus [148, 149]. In addittion, another study also showed disrupted frontolimbic connectivity and elevated local connectivity within the prefrontal cortex [137].

In particular, the new methodology developed here compares between HC participants and FTD patients, the redundancy and synergy at the triplet level, without any averaging across the ROIs involved. A methodological consequence of this choice is having

to correct for multiple existing comparisons due to the large number of triplets compared between the two groups (for 86 regions, a total of 103,340 comparisons). To overcome this problem, we have developed a clustering method similar to nonparametric threshold-free cluster enhancement (TFCE) [145]. Our clustering method, to our knowledge never used in higher interdependences studies, is the main key methodological contribution in this chapter.

At the morphological/structural level, we have found major significant atrophies in striatum, temporal pole, thalamus and amygdala, in agreement with previous findings [135, 143, 136, 146, 147, 148, 149]. On the other hand, at the level of high-order interdependences, we have found 54 triplets that have significant differences between controls and patients. Some of the ROIs in these triplets participated solely in redundancy, synergy, or both. Very striking, it is important to emphasize that, in any of the three cases, these ROIs were distributed throughout the brain specifically in differentiated regions than those where the morphological group differences were found. This suggests that our methodology, which addresses group differences in relation to high-order interdependences, is complementary to other well-established techniques in neuroimaging, such as group differences in morphological/structural MRI sequences, since the results obtained by one of the strategies cannot been reproduced by the other.

5.4 Limitations and future work

Several methodological limitations and work in progress are worth mentioning. First, we have analyzed higher-order interactions only at the triplet level due to the computational constraints of using an 86-region brain parcellation (higher orders require higher computational resources). Future work on higher interaction orders would validate the extent to which the results presented here at the triplet level are preserved at higher orders. Second, we have developed a specific clustering method with a fixed number of surrogate comparisons, but a systematic variation of this parameter and its effects on our results is needed. Third, the small sample size in this study could affect the sensitivity of the group differences found in the high order interdependences between DMF and HC. For this reason, we have preferred not to separate the DFT group into the two subgroups of svPPA and bvFTD, which, although clinically it might be interesting, a further stratification of the group would provide an even smaller sample size, which we preferred not to do that. Future work, in larger cohorts, could replicate our methodology to understand the differences between these subtypes. Fourth, our study only have focused on one fMRI preprocessing pipeline, with high international consensus in the MRI preprocessing community for connectomics, although it is well known that variations here could affect the significance of our results. Finally, the proposed methodology found a cluster of triplets with unbalanced synergy and redundancy between the two groups. The ROIs that formed the triplets had either an exclusive redundant role, an

exclusive synergistic role, or mixed participation, i.e., these ROIs were redundant in some triplets and redundant in others. Different non-parametric clustering methods, which can solve the problem of multiple comparisons in the number of triples, could be used, and future work should explore these possibilities.

5.5 Materials and Methods

5.5.1 Neuroimaging

Participants

The participants were collected from Neuroimaging in Frontotemporal Dementia (NIFD/FLTDNI). The participants enrolled in NIFD are assessed through interviews, physical examinations, and cognitive testing to characterize if each person is affected by frontotemporal lobar degeneration. We used the fMRI dataset from 75 subjects, 40 healthy controls, and 35 FTD patients: 15 participants with the behavioral variant of Frontotemporal Dementia (bvFTD), and 20 subjects with a semantic variant of a primary progressive aphasia (svPPA).

Neuroimaging pre-processing

The functional imaging preprocessing followed a similar procedure to Ref. [150]. We applied slice-time correction, and each volume was aligned to the middle volume to correct for head motion artifacts. Then, we performed a intensity normalization. Next, we regressed out 24 motion parameters, the average global signal, the average cerebrospinal fluid (CSF), and white matter signal. We applied a band-pass filter between 0.01 and 0.08 Hz and removed linear and quadratic trends. Then, all voxels were spatially smoothed with a 6 mm FWHM. Finally, we used FreeSurfer for brain segmentation and cortical parcellation. A total of 86 regions were generated, with 68 cortical regions from the Desikan-Killiany Atlas[144](34 in each hemisphere) and 18 subcortical regions (left/right thalamus, caudate, putamen, pallidum, hippocampus, amygdala, accumbens, ventral DC and cerebellum). The parcellation for each subject was projected to the individual functional data, and the mean functional time series of each region was computed.

5.5.2 Redundancy and Synergy count across group

Similar to the previous chapters, we split the O-information on positive and negative values using

$$\Omega^{+} = \max\{\Omega, 0\} \quad ; \quad \Omega^{-} = -\min\{\Omega, 0\} \ ,$$

so that $\Omega = \Omega^+ - \Omega^-$. Using these quantities, we calculated the following proxies for redundancy and synergy per subject, and triplet.

$$R_{(k)}(X_i, X_j, X_l) = \Omega^+_{(k)}(X_i, X_j, X_l) \tag{5.1}$$

$$S_{(k)}(X_i, X_j, X_l) = \Omega^-_{(k)}(X_i, X_j, X_l) \tag{5.2}$$

for $\{i, j, l\} \in \{1, \ldots, 86\}$, and $i \neq j \neq l$.
Finally, we defined the following redundancy and synergy count proxies per group and interaction order $n = 3$.

$$R_G = \big(\sum_{k=1}^{N_G} \mathbb{1}(R_{(k)}(X_1, X_2, X_3), \ldots, \sum_{k=1}^{N_G} \mathbb{1}(R_{(k)}(X_{84}, X_{85}, X_{86})\big) \tag{5.3}$$

$$S_G = \big(\sum_{k=1}^{N_G} \mathbb{1}(S_{(k)}(X_1, X_2, X_3), \ldots, \sum_{k=1}^{N_G} \mathbb{1}(S_{(k)}(X_{84}, X_{85}, X_{86})\big) \tag{5.4}$$

for $G = \{HC, FTD\}$ denoting the groups, $N_{HC} = 25$, $N_{FTD} = 35$, and $\mathbb{1}$ the indicator function,

$$\mathbb{1}(\mathbb{x}) = \begin{cases} 1, & \text{if } x \neq 0 \\ 0, & \text{otherwise.} \end{cases}$$

5.5.3 Statistical analyses

Significance of O-information values

For each subject, we first identified the values of O-information that were significantly different from zero. To do this, we generate time-shifted surrogates of the original signal with periodic boundary conditions, meaning that the tail shifting to the right of the signal is moved to the beginning of the new surrogate signal. In this way, for each of the surrogates, we preserve the mean and variance of the original signal. In particular, we implemented the following strategy:

1. We randomly chose only 10 ROIs (from the total of 86), in order to reduce computational cost.

2. For the signals corresponding to those 10 ROIs, surrogates were obtained, each one with a different time shift (min value of 1, max value of 239).

3. The O-information for all the combinations of triplets without repetition was calculated (a total of 120 combinations).

4. Steps 1-3 were repeated 100 times, obtaining the null distribution with a total number of 120*100=12,000 values of surrogate O-information.

Finally, a value of O-information is said to be significant when it is higher than two standard deviations in the null distribution, which for the Gaussian case, which is the case of our surrogate distribution, is equivalent to having a p-value less than 0.05.

Differences in redundancy and synergy per triplet

To assess whether there was an imbalance between the redundancy and synergy count of a given triplet in FTD as compared to HC, the Chi-square statistic was used. We then got a χ^2 statistic and its corresponding p-value per triplet.

Significance of clusters

Our strategy for addressing the significance of clusters resulting from the group comparisons is based on the non-parametric threshold-free cluster enhancement (TFCE) method. In particular, we followed the strategy:

1. Define a threshold τ.
2. Choose those triplets with χ^2 statistic value greater than τ.
3. Group the triplets selected in step 2 into different clusters. To do that, two triplets belong to the same cluster if they share at least one ROI in common.
4. Assign a score to each of the clusters, corresponding to the sum of the χ^2 statistic values of all triplets belonging to each cluster.
5. Calculate a p-value for each cluster using surrogates by random permutations of the labels HC and FTD. First, we calculated the surrogate χ^2 statistic values for each triplet resulting from the shuffled group comparison, and after, we repeated steps 2-4 for the new surrogate clusters. This was performed N=100 times, building the null-distribution by counting how many times the actual score was higher than the surrogate score.

This strategy was repeated for different values of τ. Our criteria for choosing the "best" threshold was to choose the τ that provided, among all significant clusters, the one with the lowest p value[1].

[1]It is important to emphasize that, due to the precise way in which we build the clusters, it is possible to obtain more than one cluster for large threshold values. However, for each threshold, we identified the lowest p-value among all clusters, thus ensuring that at least one cluster was significant, although in principle some of the other clusters might not be significant

6

Conclusions

In this thesis, we have shown how redundancy and synergy might work as informational markers to characterize changes in the high-order interactions of brain activity along the lifespan. We have used the recently proposed O-Information to quantify the intrinsic statistical synergy and the redundancy in groups of three or more interacting random variables that, in our case, were described by fMRI data. Our first result shows that the BOLD signals of older participants exhibit higher predominance of redundant interdependencies than younger participants, an effect that seems to be pervasive as is exhibited at all orders of interaction. Additionally, while there is strong heterogeneity across brain regions, we found a redundancy core at all interaction orders studied. This core is constituted by the prefrontal and motor cortices, and thus, involves working memory, executive and motor functions.

Next, to investigate the relationship between high-order functional interactions and connnectomics, we have build a neurobiologically realistic whole-brain computational model using both anatomical and functional MRI data. Our model shows that the variations in functional patterns can be explained by changes in the brain anatomical networks, which degenerate as we age. Thus, the differences in high-order functional interactions between age groups can be largely explained by variations in the connectome. Based on this finding, we propose a simple non-linear neurodegeneration model that is representative of healthy physiological aging, and that reproduces the age-variations that occur in the high-order structure of the functional data at all interaction orders, in full agreement with the empirical observations in the previous chapter. These results establish also a first step towards explaining how the reconfiguration of brain activity along the lifespan intertwines with changes in the underlying neuroanatomy.

Finally, to assess the potential of redundancy and synergy as informational markers in the pathological brain, we hypothesize that redundancy and synergy at order three might work out to assess the changes in brain activity produced by Frontotemporal Dementia. Unlike the previous chapters of this thesis, we have only focus on interaction order equal to three, because regions in this study were defined through a fine-grained

parcellation, which makes an exhaustive analysis at all orders computationally impracticable. In this chapter, we have proposed a new methodology to tackle redundancy and synergy group differences by assessing significance of clusters of triplets. As a result, we found regions that only participated in redundant interactions, other regions that only participated in synergistic interactions, and regions that participated redundantly in some triplets and synergistically in others.

Overall, the results found in this thesis begin to disentangle the complex mechanisms by which structural changes in the connectome lead to functional differences in the aging brain. Moreover, we have developed a pioneer methodology for assessing differences in the high-order interactions structure in the pathological brain. Redundancy does not only imply that the interacting areas share information, but that they share the same information. Note that no pairwise network approach could discriminate this fact.

Technically, it is important to note that our results are based on a specific fMRI preprocessing pipeline, with high consensus in the international community, but nevertheless, it could happen that some of these results could vary by changing the preprocessing pipeline. Following this possibility, we are currently working on how some variations in motion correction, part of preprocessing, affect the higher order interdependencies of the aging brain. On the other hand, to advance in the topic of neuroimaging MRI preprocessing, we are currently quantifying the integrity of the white matter tract in critically ill patients with multiple organ failure.

To conclude, I believe that we have only beginning to scratch the surface of what can be achieved with high order methods and ideas to understand the brain. In the future, I would like to extend the methodology developed in this thesis in new clinical challenges, including life expectancy, cognitive processes, neurodegenerative diseases, and psychiatric disorders.

Perspectives

An abundance of new technological advancements has enriched and enlarged experimental datasets in humans and other species, in particular in fMRI. Additionally, a wealth of novel mathematical and computational tools has emerged to help us to understand those datasets, among them novel advances in high-order statistical interdependencies among brain regions. One major factor motivating future research in high-order interactions in the brain is the characterization of these statistical interdependencies in different brain states and the understanding of the mechanistic basis of those interdependencies. We believe that future research may help to clarify the relationship of high-order interactions with our own mental capacities, perceptions, motor behavior, both in health and disease, as these mental capacities are collective properties likely to emerge beyond pairwise interactions, i.e., at high-order.

However, how best to deploy this growing experimental and analytic arsenal toward

a science based mechanistic and causal understanding of the different forms of mental functions in aging and neurodegeneration possess important challenges. It is still unclear how to choose mathematical or computational tools to capture those mechanisms. There is still a long way to go, both scientifically and transnationally to the clinics. Still few new scientific discoveries are translated into more effective treatments of mental illness. We hope that this thesis may motivate future research in this topic and novel effective treatments of mental health.
This thesis and the tools we presented open up a range of possibilities for future research. Here are some of them:

- How some variations in the movement correction of fMRI data affect the aging brain's high-order interdependencies: In this line, we are computing redundancy and synergy in data obtained following different movement correction protocols. For instance, this includes 24 head motion parameters, ICA-AROMA, both with and without global signal regression.

- To further develop the neuroimaging MRI preprocessing, we are currently quantifying the white matter tract integrity in critical patients with multiorgan failure. This longitudinal study focused on the associations between imaging and neuropsychological scores.

- Multiscale modelling and parcellations: Using different parcellations having different levels of resolution to assess high-order interdependencies.

- High order in different species: The core interest of fMRI studies to date have been understanding the human brain in health and disease. However, a key source of progress is likely to come from extending the methodology to non-human primate and rodent brains. Developments in brain recording technology move faster in animals than humans. There are openly available fMRI data for the macaque, mouse, rat, and marmoset to apply our methodologies.

- Gaussian copula approach to estimate multivariate extensions of the mutual information. In this line, we are testing different approaches to computing multivariate extensions of the mutual information, namely the total and dual total correlation. We focus our analysis on the Gaussian copulas approach.

Main achievements

First author contributions as a result of this Thesis

1. **Marilyn Gatica**, Rodrigo Cofré, Pedro A.M. Mediano, Fernando E. Rosas, Patricio Orio, Ibai Diez, S.P. Swinnen, Jesus M. Cortes. High-order interdependencies in the aging brain. Brain Connectivity, 2021 [104].

2. **Marilyn Gatica**, Fernando E. Rosas, Pedro A.M. Mediano, Ibai Diez, S.P Swinnen, Patricio Orio, Rodrigo Cofré, and Jesus M. Cortés. High-order functional interactions in aging explained via alterations in the connectome in a whole-brain model. `https://doi.org/10.1101/2021.09.15.460435` (Under Review in PLOS Computational Biology) [151].

Other publications

1. Patricio Orio, **Marilyn Gatica**, Rubén Herzog, Jean Paul Maidana, Samy Castro, Kesheng Xu, Chaos versus noise as drivers of multistability in neural networks, Chaos: An Interdisciplinary Journal of Nonlinear Science, 28, 106321, 2018 [152].

In Preparation

1. **Marilyn Gatica**, Itziar Benito-Sanchez, Antonio Jimenez-Marin, Borja Camino-Pontes, Diego Rivera, Daniela Ramos-Usuga, Victoria Boado, Fermin Labayen, Alberto Cabrera, Juan Carlos Arango-Lasprilla, and Jesus M. Cortés. Longitudinal alterations in brain connectivity after multiorgan failure and their association with cognitive performance.

2. Pedro Mediano, **Marilyn Gatica**, Ruben Herzog, and Rodrigo Cofré. Gaussian copula approach to estimate multivariate extensions of the mutual information.

Software contributions

The code to compute the metrics used in this thesis (Redundancy, Synergy, O-information, and S-information) has been made publicly available at `www.github.com/brincolab/High-Order-interactions`.

Funding and award

- Fellowship CONICYT-PFCHA/Doctorado Nacional/2019-21190577, 2019-2022.
- Award for best oral exposition. XV Annual Meeting of the Chilean Society for Neuroscience 2019, La Serena, Chile.

- Conference fellowship to XV Annual Meeting of the Chilean Society for Neuroscience 2019, La Serena, Chile.
- Fellowship FIB-UV, 2018.

Outreach

- Interview at Radio Usach. Dissemination of our article High-order interdependencies in the aging brain. `https://www.youtube.com/watch?v=TgRN7YPaZoQ&t=1431s`, min. 10:20.
- Online presentation in Commemoration of International Women's Day. The maths of aging. `https://www.youtube.com/watch?v=CLwTB_MlPzg&t=3349s`, min. 36:20.

Teaching

- Part-time lecturer at Computational Neuroscience in Python, Spring 2018/2020, Universidad de Santiago de Chile. Course to Mathematical Engineering students.
- Part-time lecturer at Introduction to Mathematical Engineering , Fall 2019/2020, Universidad de Santiago de Chile. Course to 1st year Mathematical Engineering students.

Appendix A: Supplementary figures

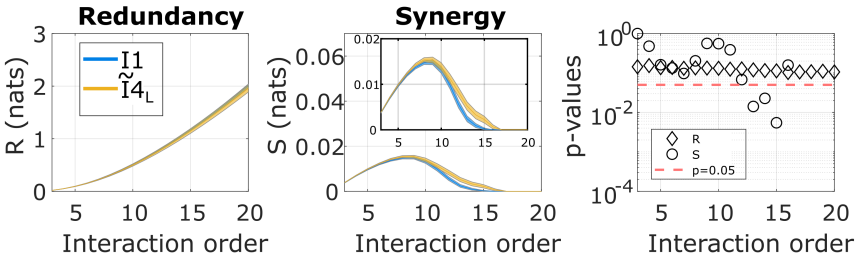

Figure S1: **The linear aging model does not provide significant differences in redundancy between age groups**. Similar to Fig. 3C in the main text, but for a synthetic I4 age group using a linear model ($\tilde{\mathrm{I}}4_L$) for aging instead of a quadratic one. Redundancy (left) and synergy (middle) are plotted as a function of interaction order and then, for each interaction order, Wilcoxon rank-sum test p-values are obtained after comparing their values between the groups $\tilde{\mathrm{I}}4_L$ and I1. If the p-values survived the FDR multiple comparison correction, both the diamonds and the circles were filled in.

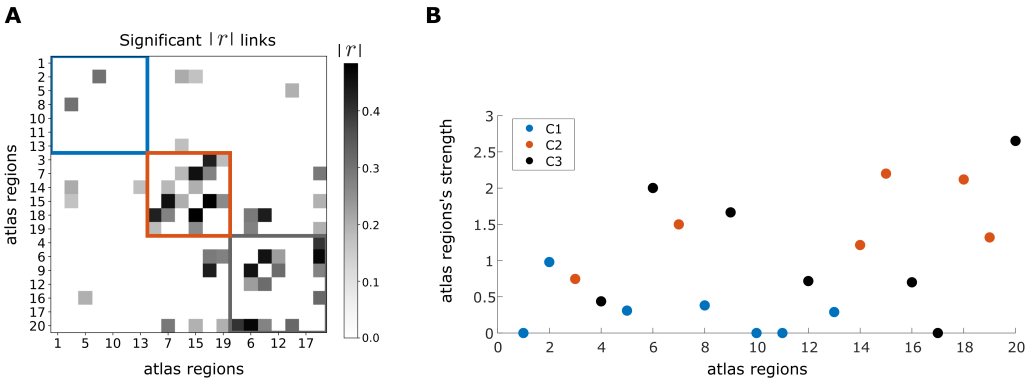

Figure S2: **Node strength values across different nodes communities (C) affected by age.** Nodes here are atlas regions. **A:** Rate degeneration matrix calculated using the absolute values of r, and where all links in the matrix survived to Bonferroni correction (a similar matrix was shown in the right panel of Figure 4 of the main manuscript). **B:** Strength values for all atlas regions (nodes) calculated on the rate degeneration matrix show in panel A. Node strength was calculated by summing over all positive values in each row or column in the matrix. **A,B:** Colors blue (C1), orange (C2) and black (C3) indicate different communities.

Appendix B: Introductory probability concepts

Definition 4 *Let Ω be a non-empty subset. A class of Ω subsets, denoted by $\mathfrak{F}$, is called σ-algebra of Ω if satisfying:*

1. $\emptyset \in \mathfrak{F}$
2. *If $A \in \mathfrak{F}$, then $A^c \in \mathfrak{F}$*
3. *If $A_n \in \mathfrak{F}$ for all $n \in \mathbb{N}$, then $\bigcup_{n=1}^{\infty} A_n \in \mathfrak{F}$.*

Definition 5 *The Borel σ-algebra of $\mathbb{R}$, denoted by $\mathcal{B}(\mathbb{R})$, is the minor σ-algebra containing all the open intervals of $\mathbb{R}$.*

Definition 6 *Let Ω be a non-empty space and $\mathfrak{F}$ a σ-algebra of Ω. Then, measurable space is defined as the tuple $(\Omega, \mathfrak{F})$.*

Definition 7 *Let $(\Omega, \mathfrak{F})$ be a measurable space. G is called a sub-σ-algebra of $\mathfrak{F}$ if G is a σ-algebra of Ω and $G\mathfrak{F}$.*

Definition 8 *Let $(\Omega, \mathfrak{F})$ be a measurable space. Then, $\mu : \Omega \to [0, \infty]$ is called a measure of $(\Omega, \mathfrak{F})$ if it satisfies the following properties:*

1. $\mu(\emptyset) = 0$.
2. *For all $A \in \mathfrak{F}$, $\mu(A) \geq 0$.*
3. *(σ-**additivity**) For all sequence of disjoint sets $A_i \in \mathfrak{F}$, $i \in \mathbb{N}$:*

$$\mu(\bigcup_{n=1}^{\infty}) = \sum_{n=1}^{\infty} \mu(A_n).$$

Definition 9 *Let Ω be a non-empty space, $\mathfrak{F}$ a σ-algebra of Ω, and μ a measure of $(\Omega, \mathfrak{F})$. Then, the triplet $(\Omega, \mathfrak{F}, \mu)$ is called a measure space.*

Definition 10 *A probability space is a measure space $(\Omega, \mathfrak{F}, \mathbb{P})$, where the measure over $(\Omega, \mathfrak{F})$ satisfying $\mathbb{P}(\Omega = 1)$.*

The introductory mathematical concepts from measurement theory are in appendix A.

Definition 11 *Let $(\Omega, \mathfrak{F}, \mathbb{P})$ be a probability space. A* **random variable** *X is a function $X : \Omega \to \mathbb{R}$ such that $X^{-1}(A) \in \mathfrak{F}$, for all $A \in \mathcal{B}(\mathbb{R})$. That is:*

$$\mathbb{P}\{X \in A\} = \mathbb{P}(X^{-1}(A)).$$

Definition 12 *The* **cumulative density function (CDF)** *F of the random variable X is defined for any real number x by:*

$$F(x) = \mathbb{P}\{X \leq x\} = \mathbb{P}\{X \in (-\infty, x])\}.$$

Then, $\overline{F}(x) \coloneqq 1 - F(x) = \mathbb{P}\{X > x\}$

Definition 13 *A random variable X is said to be* **discrete** *if its set of possible values is countable. Moreover, for discrete random variables*

$$F(x) = \sum_{x \leq y} \mathbb{P}\{X = y\} = \sum_{x \leq y} p(y),$$

where p is the probability mass function. Notice that, p is a function that gives the probability that a discrete random variable is exactly equal to some value.

Definition 14 *A random variable X is said to be* **continuous** *if there exists a function f, called the* **probability density function (PDF)**, *such that:*

$$\mathbb{P}\{a \leq X \leq b\} = \int_a^b f(x)\, dx.$$

Hence, if F is the CDF of X,

$$F(x) = \int_{-\infty}^{x} f(s)\, ds,$$

and it follows $f(x) = \frac{d}{dx} F(x)$ (fundamental theorem of calculus).

Definition 15 *The* **expectation** *or mean of the random variable X, denoted by $\mathbb{E}[X]$, is defined by:*

$$\begin{aligned} \mathbb{E}[X] &= \int_{-\infty}^{\infty} x\, dF(x) \\ &= \begin{cases} \int_{-\infty}^{\infty} x f(x)\, dx & \text{if } X \text{ is continuous,} \\ \sum_x x \mathbb{P}\{X = x\} & \text{if } X \text{ is discrete.} \end{cases} \end{aligned}$$

In general terms, for any function of X, say $h(X)$:

$$\mathbb{E}[h(X)] = \int_{-\infty}^{\infty} x\, dF_h(x),$$

where $F_h(X)$ is the distribution function of the random variable $h(X)$.

Bibliography

[1] World Health Organization. Ageing and health. https://www.who.int/news-room/fact-sheets/detail/ageing-and-health, 2018.

[2] United Nations Dept. Economic and Population Division Social Affairs. World Population Ageing 2020 Highlights: Living arrangements of older persons. United Nations, ST/ESA/SER.A/451, 2020.

[3] Anna A Kondratova and Roman V Kondratov. The circadian clock and pathology of the ageing brain. Nature Reviews. Neuroscience, 13(5):325–335, 2012.

[4] Cheryl Grady. The cognitive neuroscience of ageing. Nature Reviews Neuroscience, 13(7):491–505, 2012.

[5] Bob G Knight and Kelly Durbin. Aging and the effects of emotion on cognition: Implications for psychological interventions for depression and anxiety. PsyCh Journal, 4(1):11–19, 2015.

[6] Hedieh Sajedi and Nastaran Pardakhti. Age Prediction Based on Brain MRI Image: A Survey. Journal of Medical Systems, 2019.

[7] Jonas Persson, Lars Nyberg, Johanna Lind, Anne Larsson, Lars Göran Nilsson, Martin Ingvar, and Randy L Buckner. Structure-function correlates of cognitive decline in aging. Cerebral Cortex, 2006.

[8] J S Damoiseaux, C F Beckmann, E J.Sanz Arigita, F Barkhof, Ph Scheltens, C J Stam, S M Smith, and S A R B Rombouts. Reduced resting-state brain activity in the "default network" in normal aging. Cerebral Cortex, 2008.

[9] Ian J Deary, Janie Corley, Alan J Gow, Sarah E Harris, Lorna M Houlihan, Riccardo E Marioni, Lars Penke, Snorri B Rafnsson, and John M Starr. Age-associated cognitive decline. British Medical Bulletin, 2009.

[10] Luiz Kobuti Ferreira and Geraldo F Busatto. Resting-state functional connectivity in normal brain aging. Neuroscience and Biobehavioral Reviews, 2013.

[11] Anira Escrichs, Carles Biarnes, Josep Garre-Olmo, José Manuel Fernández-Real, Rafel Ramos, Reinald Pamplona, Ramon Brugada, Joaquin Serena, Lluís Ramió-Torrentà, Gabriel Coll-De-Tuero, Luís Gallart, Jordi Barretina, Joan C Vilanova, Jordi Mayneris-Perxachs, Marco Essig, Chase R Figley, Salvador Pedraza, Josep

Puig, and Gustavo Deco. Whole-Brain Dynamics in Aging: Disruptions in Functional Connectivity and the Role of the Rich Club. Cerebral Cortex, 2021.

[12] M. Symms, H. R. Jäger, K. Schmierer, and T. A. Yousry. A review of structural magnetic resonance neuroimaging, 2004.

[13] S. Ogawa, T. M. Lee, A. R. Kay, and D. W. Tank. Brain magnetic resonance imaging with contrast dependent on blood oxygenation. Proceedings of the National Academy of Sciences of the United States of America, 1990.

[14] Ludovica Griffanti, Gwenaëlle Douaud, Janine Bijsterbosch, Stefania Evangelisti, Fidel Alfaro-Almagro, Matthew F. Glasser, Eugene P. Duff, Sean Fitzgibbon, Robert Westphal, Davide Carone, Christian F. Beckmann, and Stephen M. Smith. Hand classification of fMRI ICA noise components. NeuroImage, 2017.

[15] Linden Parkes, Ben Fulcher, Murat Yücel, and Alex Fornito. An evaluation of the efficacy, reliability, and sensitivity of motion correction strategies for resting-state functional MRI. NeuroImage, 2018.

[16] fMRIPrep: a robust preprocessing pipeline for functional MRI. Nature Methods, 2019.

[17] Mark Jenkinson and Michael Chappell. Introduction to neuroimaging analysis . 2018.

[18] E Courchesne, H J Chisum, J Townsend, A Cowles, J Covington, B Egaas, M Harwood, S Hinds, and G A Press. Normal brain development and aging: Quantitative analysis at in vivo MR imaging in healthy volunteers. Radiology, 2000.

[19] Mark J West. Regionally specific loss of neurons in the aging human hippocampus. Neurobiology of Aging, 1993.

[20] Edith V Sullivan, Torsten Rohlfing, and Adolf Pfefferbaum. Quantitative fiber tracking of lateral and interhemispheric white matter systems in normal aging: Relations to timed performance. Neurobiology of Aging, 2010.

[21] M P Boisgontier, P van Ruitenbeek, I Leunissen, S Chalavi, S Sunaert, O Levin, and S P Swinnen. Nucleus accumbens and caudate atrophy predicts longer action selection times in young and old adults. Hum Brain Mapp, 37:4629–4639, 2016.

[22] S Chalavi, H Z Adab, L Pauwels, I A M Beets, P van Ruitenbeek, M P Boisgontier, T S Monteiro, C Maes, S Sunaert, and S P Swinnen. Anatomy of Subcortical Structures Predicts Age-Related Differences in Skill Acquisition. Cereb Cortex, 28:459–473, 2018.

[23] T L Jernigan, S L Archibald, C Fennema-Notestine, A C Gamst, J C Stout, J Bonner, and J R Hesselink. Effects of age on tissues and regions of the cerebrum and cerebellum. Neurobiol Aging, 2001.

[24] Maria Grazia Puxeddu, Joshua Faskowitz, Richard F Betzel, Manuela Petti, Laura Astolfi, and Olaf Sporns. The modular organization of brain cortical connectivity across the human lifespan. NeuroImage, 2020.

[25] Mikail Rubinov and Olaf Sporns. Complex network measures of brain connectivity: Uses and interpretations. NeuroImage, 52(3):1059–1069, 2010.

[26] G Tononi, O Sporns, and G M Edelman. A measure for brain complexity: relating functional segregation and integration in the nervous system. Proceedings of the National Academy of Sciences, 1994.

[27] Miao Cao, Jin Hui Wang, Zheng Jia Dai, Xiao Yan Cao, Li Li Jiang, Feng Mei Fan, Xiao Wei Song, Ming Rui Xia, Ni Shu, Qi Dong, Michael P. Milham, F. Xavier Castellanos, Xi Nian Zuo, and Yong He. Topological organization of the human brain functional connectome across the lifespan. Developmental Cognitive Neuroscience, 2014.

[28] Emily L. Dennis, Neda Jahanshad, Katie L. McMahon, Greig I. de Zubicaray, Nicholas G. Martin, Ian B. Hickie, Arthur W. Toga, Margaret J. Wright, and Paul M. Thompson. Development of brain structural connectivity between ages 12 and 30: A 4-Tesla diffusion imaging study in 439 adolescents and adults. NeuroImage, 2013.

[29] Hao Huang, Ni Shu, Virendra Mishra, Tina Jeon, Lina Chalak, Zhiyue J. Wang, Nancy Rollins, Gaolang Gong, Hua Cheng, Yun Peng, Qi Dong, and Yong He. Development of human brain structural networks through infancy and childhood. Cerebral Cortex, 2015.

[30] Naftali Raz, Ulman Lindenberger, Karen M Rodrigue, Kristen M Kennedy, Denise Head, Adrienne Williamson, Cheryl Dahle, Denis Gerstorf, and James D Acker. Regional brain changes in aging healthy adults: General trends, individual differences and modifiers. Cerebral Cortex, 2005.

[31] Luiz Kobuti Ferreira, Ana Carolina Brocanello Regina, Natasa Kovacevic, Maria Da Graça Morais Martin, Pedro Paim Santos, Camila De Godoi Carneiro, Daniel Shikanai Kerr, Edson Amaro, Anthony Randal Mcintosh, and Geraldo F Busatto. Aging effects on whole-brain functional connectivity in adults free of cognitive and psychiatric disorders. Cerebral Cortex, 2016.

[32] Eleanna Varangis, Christian G Habeck, Qolamreza R Razlighi, and Yaakov Stern. The Effect of Aging on Resting State Connectivity of Predefined Networks in the Brain. Frontiers in Aging Neuroscience, 2019.

[33] Joana Cabral, Morten L Kringelbach, and Gustavo Deco. NeuroImage Functional connectivity dynamically evolves on multiple time-scales over a static structural connectome : Models and mechanisms. NeuroImage, (March):0–1, 2017.

[34] Enrique C A Hansen, Demian Battaglia, Andreas Spiegler, Gustavo Deco, and Viktor K Jirsa. NeuroImage Functional connectivity dynamics : Modeling the switching behavior of the resting state. NeuroImage, 105:525–535, 2015.

[35] Nora Leonardi, Jonas Richiardi, Markus Gschwind, Samanta Simioni, Jean-marie Annoni, Myriam Schluep, Patrik Vuilleumier, and Dimitri Van De Ville. NeuroImage Principal components of functional connectivity : A new approach to study dynamic brain connectivity during rest. NeuroImage, 83:937–950, 2013.

[36] Patricio Orio, Marilyn Gatica, Rubén Herzog, Jean Paul Maidana, Samy Castro, and Kesheng Xu. Chaos versus noise as drivers of multistability in neural networks. Chaos, 2018.

[37] Maria Giulia Preti, Thomas A W Bolton, and Dimitri Van De Ville. The dynamic functional connectome: State-of-the-art and perspectives. NeuroImage, 2017.

[38] Diego Vidaurre, Andrew J. Quinn, Adam P. Baker, David Dupret, Alvaro Tejero-Cantero, and Mark W. Woolrich. Spectrally resolved fast transient brain states in electrophysiological data. NeuroImage, 2016.

[39] Jessica R Andrews-Hanna, Abraham Z Snyder, Justin L Vincent, Cindy Lustig, Denise Head, Marcus E E Raichle, and Randy L Buckner. Disruption of Large-Scale Brain Systems in Advanced Aging. Neuron, 2007.

[40] Lauren E Mak, Luciano Minuzzi, Glenda MacQueen, Geoffrey Hall, Sidney H Kennedy, and Roumen Milev. The Default Mode Network in Healthy Individuals: A Systematic Review and Meta-Analysis. Brain Connectivity, 2017.

[41] Richard F. Betzel, Lisa Byrge, Ye He, Joaquín Goñi, Xi Nian Zuo, and Olaf Sporns. Changes in structural and functional connectivity among resting-state networks across the human lifespan. NeuroImage, 102(P2):345–357, 2014.

[42] Anders M Fjell, Markus H Sneve, Andreas B Storsve, Håkon Grydeland, Anastasia Yendiki, and Kristine B Walhovd. Brain Events Underlying Episodic Memory Changes in Aging: A Longitudinal Investigation of Structural and Functional Connectivity. Cerebral Cortex, 2016.

[43] Cheryl Grady, Saman Sarraf, Cristina Saverino, and Karen Campbell. Age differences in the functional interactions among the default, frontoparietal control, and dorsal attention networks. Neurobiology of Aging, 41:159–172, 2016.

[44] Linda Geerligs, Remco J Renken, Emi Saliasi, Natasha M Maurits, and Monicque M Lorist. A Brain-Wide Study of Age-Related Changes in Functional Connectivity. Cerebral Cortex, 2015.

[45] B R King, P van Ruitenbeek, I Leunissen, K Cuypers, K F Heise, T Santos Monteiro, L Hermans, O Levin, G Albouy, D Mantini, and S P Swinnen. Age-Related Declines in Motor Performance are Associated With Decreased Segregation of Large-Scale Resting State Brain Networks. Cereb Cortex, 28:4390–4402, 2018.

[46] T S Monteiro, B R King, Adab H Zivari, D Mantini, and S P Swinnen. Age-related differences in network flexibility and segregation at rest and during motor performance. Neuroimage, 194:93–104, 2019.

[47] Karl J Friston and Cathy J Price. Degeneracy and redundancy in cognitive anatomy. Trends in Cognitive Sciences, 7(4):151–152, 2003.

[48] Elad Schneidman, William Bialek, and Michael J. Berry. Synergy, Redundancy, and Independence in Population Codes. The Journal of Neuroscience, 2003.

[49] Asier Erramuzpe, Guillermo J Ortega, Jesus Pastor, Rafael G.De Sola, Daniele Marinazzo, Sebastiano Stramaglia, and Jesus M Cortes. Identification of redundant and synergetic circuits in triplets of electrophysiological data. Journal of Neural Engineering, 12(6), 2015.

[50] Sebastiano Stramaglia, Leonardo Angelini, Guorong Wu, Jesus M. Cortes, Luca Faes, and Daniele Marinazzo. Synergetic and Redundant Information Flow Detected by Unnormalized Granger Causality: Application to Resting State fMRI. IEEE Transactions on Biomedical Engineering, 63(12):2518–2524, 2016.

[51] Robin A A Ince. Measuring multivariate redundant information with pointwise common change in surprisal. Entropy, 19(7), 2017.

[52] Robin A.A. Ince, Bruno L. Giordano, Christoph Kayser, Guillaume A. Rousselet, Joachim Gross, and Philippe G. Schyns. A statistical framework for neuroimaging data analysis based on mutual information estimated via a gaussian copula. Human Brain Mapping, 38(3):1541–1573, 2017.

[53] Fernando Rosas, Pedro A M Mediano, Mart\'\in Ugarte, and Henrik J Jensen. An information-theoretic approach to self-organisation: Emergence of complex interdependencies in coupled dynamical systems. Entropy, 20(10):793, 2018.

[54] Fernando Rosas, Pedro A. M. Mediano, Michael Gastpar, and Henrik J. Jensen. Quantifying High-order Interdependencies via Multivariate Extensions of the Mutual Information. Physical Review E, 100(3):32305, 2019.

[55] Nicholas Timme, Wesley Alford, Benjamin Flecker, and John M. Beggs. Synergy, redundancy, and multivariate information measures: An experimentalist's perspective. Journal of Computational Neuroscience, 36(2):119–140, 2014.

[56] Andrea I Luppi, Pedro A M Mediano, Fernando E Rosas, Negin Holland, Tim D Fryer, John T O'Brien, James B Rowe, David K Menon, Daniel Bor, and Emmanuel A Stamatakis. A synergistic core for human brain evolution and cognition. BioRxiv, 2020.

[57] Giulio Tononi and Gerald M Edelman. Consciousness and complexity. science, 282(5395):1846–1851, 1998.

[58] Borja Camino-Pontes, Ibai Diez, Antonio Jimenez-Marin, Javier Rasero, Asier Erramuzpe, Paolo Bonifazi, Sebastiano Stramaglia, Stephan Swinnen, and Jesus Cortes. Interaction Information Along Lifespan of the Resting Brain Dynamics Reveals a Major Redundant Role of the Default Mode Network. Entropy, 20(10):742, sep 2018.

[59] Yoav Benjamini and Yosef Hochberg. Controlling the false discovery rate: a practical and powerful approach to multiple testing. Journal of the Royal statistical society: series B (Methodological), 57(1):289–300, 1995.

[60] Jessica R. Andrews-Hanna, Abraham Z. Snyder, Justin L. Vincent, Cindy Lustig, Denise Head, Marcus E. Raichle, and Randy L. Buckner. Disruption of Large-Scale Brai Systems in Advanced Aging. Neuron, 56(5):924–935, December 2007.

[61] Micaela Y. Chan, Denise C. Park, Neil K. Savalia, Steven E. Petersen, and Gagan S. Wig. Decreased segregation of brain systems across the healthy adult lifespan. Proceedings of the National Academy of Sciences of the United States of America, 111(46):E4997–E5006, nov 2014.

[62] Keiichi Onoda, Masaki Ishihara, and Shuhei Yamaguchi. Decreased functional connectivity by aging is associated with cognitive decline. Journal of cognitive neuroscience, 2012.

[63] Elena Solesio-Jofre, Leen Serbruyns, Daniel G Woolley, Dante Mantini, Iseult A M Beets, and Stephan P Swinnen. Aging effects on the resting state motor network and interlimb coordination. Human Brain Mapping, 2014.

[64] Federico Battiston, Giulia Cencetti, Iacopo Iacopini, Vito Latora, Maxime Lucas, Alice Patania, Jean Gabriel Young, and Giovanni Petri. Networks beyond pairwise interactions: Structure and dynamics, 2020.

[65] Sebastiano Stramaglia, Tomas Scagliarini, Bryan C. Daniels, and Daniele Marinazzo. Quantifying Dynamical High-Order Interdependencies From the O-Information: An Application to Neural Spiking Dynamics. Frontiers in Physiology, 2021.

[66] Paul L Williams and Randall D Beer. Nonnegative decomposition of multivariate information. arXiv preprint arXiv:1004.2515, 2010.

[67] William J McGill. Multivariate information transmission. IRE Professional Group on Information Theory, 1954.

[68] Michael Wibral, Viola Priesemann, Jim W Kay, Joseph T Lizier, and William A Phillips. Partial information decomposition as a unified approach to the specification of neural goal functions. Brain and cognition, 112:25–38, 2017.

[69] Andrea I Luppi, Pedro A M Mediano, Fernando E Rosas, Judith Allanson, John D Pickard, Robin L Carhart-Harris, Guy B Williams, Michael M Craig, Paola Finoia, Adrian M Owen, and Others. A synergistic workspace for human consciousness revealed by integrated information decomposition. BioRxiv, 2020.

[70] I Diez, P Bonifazi, I Escudero, B Mateos, M A Muñoz, S Stramaglia, and J M Cortes. A novel brain partition highlights the modular skeleton shared by structure and function. Scientific Reports, 5:10532, 2015.

[71] Ibai Diez, David Drijkoningen, Sebastiano Stramaglia, Paolo Bonifazi, Daniele Marinazzo, Jolien Gooijers, Stephan P Swinnen, and Jesus M Cortes. Enhanced prefrontal functional–structural networks to support postural control deficits after traumatic brain injury in a pediatric population. Network Neuroscience, 1(2):116–142, 2017.

[72] C L Grady. Cognitive neuroscience of aging. Ann N Y Acad Sci, 1124:127–144, 2008.

[73] D G Salat, R L Buckner, A Z Snyder, D N Greve, R S Desikan, E Busa, J C Morris, A M Dale, and B Fischl. Thinning of the cerebral cortex in aging. Cereb Cortex, 14:721–730, 2004.

[74] L Pauwels, C Maes, L Hermans, and S P Swinnen. Motor inhibition efficiency in healthy aging: the role of gamma-aminobutyric acid. Neural Regen Res, 14:741–744, 2019.

[75] S Heuninckx, N Wenderoth, and S P Swinnen. Systems neuroplasticity in the aging brain: recruiting additional neural resources for successful motor performance in elderly persons. J Neurosci, 28(1):91–99, 2008.

[76] T Santos-Monteiro, I A M Beets, M P Boisgontier, J Gooijers, L Pauwels, S Chalavi, B King, G Albouy, and S P Swinnen. Relative cortico-subcortical shift in brain activity but preserved training-induced neural modulation in older adults during bimanual motor learning. Neurobiol Aging, 58:54–67, 2017.

[77] L M Rueda-Delgado, K F Heise, A Daffertshofer, D Mantini, and S P Swinnen. Age-related differences in neural spectral power during motor learning. Neurobiol Aging, 77:44–57, 2019.

[78] S Heuninckx, N Wenderoth, F Debaere, R Peeters, and S P Swinnen. Neural basis of aging: the penetration of cognition into action control. J Neurosci, 25:6787–6796, 2005.

[79] M E Raichle. The brain's default mode network. Annu Rev Neurosci, 38:433–447, 2015.

[80] R L Buckner, J R Andrews-Hanna, and D L Schacter. The brain's default network: anatomy, function, and relevance to disease. Ann N Y Acad Sci, 1124:1–38, 2008.

[81] D S Margulies, J L Vincent, C Kelly, G Lohmann, L Q Uddin, B B Biswal, A Villringer, F X Castellanos, M P Milham, and M Petrides. Precuneus shares intrinsic functional architecture in humans and monkey. Proc Natl Acad Sci U S A, 106:20069–20074, 2009.

[82] C F Beckmann, M DeLuca, J T Devlin, and S M Smith. Investigations into resting-state connectivity using independent component analysis. Philos Trans R Soc Lond B Biol Sci, 360:1001–1013, 2005.

[83] A P Schultz, J P Chhatwal, T Hedden, E C Mormino, B J Hanseeuw, J Sepulcre, W Huijbers, M LaPoint, R F Buckley, K A Johnson, and R A Sperling. Phases of Hyperconnectivity and Hypoconnectivity in the Default Mode and Salience Networks Track with Amyloid and Tau in Clinically Normal Individuals. J Neurosci, 37:4323–4331, 2017.

[84] K Abbas, T E Shenk, V N Poole, E L Breedlove, L Z Leverenz, E A Nauman, T M Talavage, and M E Robinson. Alteration of default mode network in high school football athletes due to repetitive subconcussive mild traumatic brain injury: a resting-state functional magnetic resonance imaging study. Brain Connect, 5:91–101, 2015.

[85] A Jimenez-Marina, D Rivera, V Boado, I Diez, F Labayen, I Garrido, D Ramos-Usuga, I Benito-Sanchez, J Rasero, A Cabrera-Zubizarreta, I Gabilondo, S Stramaglia, J C Arango-Lasprilla, and J M Cortes. Brain connectivity and cognitive functioning in individuals six months after multiorgan failure. NeuroImage: Clinical, 25:102137, 2020.

[86] Joseph T Lizier, Nils Bertschinger, Juergen Jost, and Michael Wibral. Information decomposition of target effects from multi-source interactions: Perspectives on previous, current and futurework. Entropy, 2018.

[87] Javier Rasero, Carmen Alonso-Montes, Ibai Diez, Laiene Olabarrieta-Landa, Lakhdar Remaki, Iñaki Escudero, Beatriz Mateos, Paolo Bonifazi, Manuel Fernandez, Juan Carlos Arango-Lasprilla, Sebastiano Stramaglia, Jesus M Cortes, and the Alzheimer's Disease Neuroimaging Initiative. Group-Level Progressive Alterations in Brain Connectivity Patterns Revealed by Diffusion-Tensor Brain Networks across Severity Stages in Alzheimer's Disease. Frontiers in Aging Neuroscience, 9:215, 2017.

[88] Changchun He, Huafu Chen, Lucina Q Uddin, Asier Erramuzpe, Paolo Bonifazi, Xiaonan Guo, Jinming Xiao, Heng Chen, Xinyue Huang, Lei Li, Wei Sheng, Wei Liao, Jesus M Cortes, and Xujun Duan. Structure–Function Connectomics Reveals Aberrant Developmental Trajectory Occurring at Preadolescence in the Autistic Brain. Cerebral Cortex, 30(9):5028–5037, 2020.

[89] Izaro Fernandez-Iriondo, Antonio Jimenez-Marin, Ibai Diez, Paolo Bonifazi, Stephan P Swinnen, Miguel A Muñoz, and Jesus M Cortes. Small variation in dynamic functional connectivity in cerebellar networks. Neurocomputing, 2021.

[90] Paolo Bonifazi, Asier Erramuzpe, Ibai Diez, Iñigo Gabilondo, Matthieu P Boisgontier, Lisa Pauwels, Sebastiano Stramaglia, Stephan P Swinnen, and Jesus M Cortes. Structure–function multi-scale connectomics reveals a major role of the fronto-striato-thalamic circuit in brain aging. Human Brain Mapping, 39(12):4663–4677, 2018.

[91] Gustavo Deco and Morten L Kringelbach. Great expectations: using whole-brain computational connectomics for understanding neuropsychiatric disorders. Neuron, 84(5):892–905, 2014.

[92] Gustavo Deco, Josephine Cruzat, Joana Cabral, Gitte M Knudsen, Robin L Carhart-Harris, Peter C Whybrow, Nikos K Logothetis, and Morten L Kringelbach. Whole-brain multimodal neuroimaging model using serotonin receptor maps explains non-linear functional effects of lsd. Current biology, 28(19):3065–3074, 2018.

[93] Rodrigo Cofré, Rubén Herzog, Pedro A M Mediano, Juan Piccinini, Fernando E Rosas, Yonatan Sanz Perl, and Enzo Tagliazucchi. Whole-brain models to explore altered states of consciousness from the bottom up. Brain Sciences, 2020.

[94] Gustavo Deco and Viktor K Jirsa. Ongoing cortical activity at rest: Criticality, multistability, and ghost attractors. Journal of Neuroscience, 2012.

[95] Yi Feng Wang, Feng Liu, Zhi Liang Long, Xu Jun Duan, Qian Cui, Jin H. Yan, and Hua Fu Chen. Steady-State BOLD Response Modulates Low Frequency Neural Oscillations. Scientific Reports, 4:4–10, 2014.

[96] Enrique C A Hansen, Demian Battaglia, Andreas Spiegler, Gustavo Deco, and Viktor K Jirsa. Functional connectivity dynamics: modeling the switching behavior of the resting state. Neuroimage, 105:525–535, 2015.

[97] E Bisiach and C Luzzatti. Unilateral neglect of representational space. Cortex, 1978.

[98] W B Scoville and B Milner. Loss of recent memory after bilateral hippocampal lesions. Journal of neurology, neurosurgery, and psychiatry, 1957.

[99] Jessica R Newton and Mriganka Sur. Rewiring Cortex: Functional Plasticity of the Auditory Cortex during Development. Plasticity and Signal Representation in the Auditory System, 2006.

[100] Joana Cabral, Morten L Kringelbach, and Gustavo Deco. Exploring the network dynamics underlying brain activity during rest. Progress in Neurobiology, 114:102–131, 2014.

[101] Joana Cabral, Morten L Kringelbach, and Gustavo Deco. Functional connectivity dynamically evolves on multiple time-scales over a static structural connectome: Models and mechanisms. NeuroImage, 160:84–96, 2017.

[102] Rubén Herzog, Pedro A M Mediano, Fernando E Rosas, Robin Carhart-Harris, Yonatan Sanz Perl, Enzo Tagliazucchi, and Rodrigo Cofre. A mechanistic model of the neural entropy increase elicited by psychedelic drugs. Scientific Reports, 2020.

[103] K J Friston, A Mechelli, R Turner, and C J Price. Nonlinear responses in fMRI: The balloon model, Volterra kernels, and other hemodynamics. NeuroImage, 2000.

[104] Marilyn Gatica, Rodrigo Cofre, Pedro A M Mediano, Fernando E Rosas, Patricio Orio, Ibai Diez, S P Swinnen, and Jesus M Cortes. High-order interdependencies in the aging brain. Brain Connectivity, 2021.

[105] Paul L Williams and Randall D Beer. Nonnegative decomposition of multivariate information. arXiv preprint arXiv:1004.2515, 2010.

[106] Carlos Coronel-Oliveros, Rodrigo Cofré, and Patricio Orio. Cholinergic neuromodulation of inhibitory interneurons facilitates functional integration in whole-brain models. PLoS Computational Biology, 2021.

[107] Carlos Coronel-Oliveros, Samy Castro, Rodrigo Cofré, and Patricio Orio. Structural Features of the Human Connectome That Facilitate the Switching of Brain Dynamics via Noradrenergic Neuromodulation. Frontiers in Computational Neuroscience, 15, 2021.

[108] Andrea I Luppi, Pedro A M Mediano, Fernando E Rosas, Judith Allanson, John D Pickard, Guy B Williams, Michael M Craig, Paola Finoia, Alexander R D Peattie, Peter Coppola, Adrian Owen, Lorina Naci, David K Menon, Daniel Bor, and Emmanuel A Stamatakis. Paths to Oblivion: Common Neural Mechanisms of Anaesthesia and Disorders of Consciousness. bioRxiv, 2021.

[109] Gustavo Deco, Josephine Cruzat, Joana Cabral, Enzo Tagliazucchi, Helmut Laufs, Nikos K Logothetis, and Morten L Kringelbach. Awakening: Predicting external stimulation to force transitions between different brain states. Proceedings of the National Academy of Sciences of the United States of America, 2019.

[110] Jennifer S Goldman, Lionel Kusch, Bahar Hazal Yalcinkaya, Damien Depannemaecker, Trang-Anh E Nghiem, Viktor Jirsa, and Alain Destexhe. Brain-scale emergence of slow-wave synchrony and highly responsive asynchronous states based on biologically realistic population models simulated in The Virtual Brain. bioRxiv, 2020.

[111] A Rasooli, Adab H Zivari, S Chalavi, T S Monteiro, T Dhollander, D Mantini, and S P Swinnen. Prefronto-Striatal Structural Connectivity Mediates Adult Age Differences in Action Selection. J Neurosci, 41:331–341, 2020.

[112] J P Coxon, A Van Impe, N Wenderoth, and Swinnen SP. Aging and inhibitory control of action: cortico-subthalamic connection strength predicts stopping performance. J Neurosci, 32:8401–8412, 2012.

[113] M Ystad, E Hodneland, S Adolfsdottir, J Haász, A J Lundervold, T Eichele, and A Lundervold. Cortico-striatal connectivity and cognition in normal aging: a combined DTI and resting state fMRI study. Neuroimage, 55:24–31, 2011.

[114] J Golomb, M J de Leon, A Kluger, A E George, C Tarshish, and S H Ferris. Hippocampal Atrophy in Normal Aging: An Association With Recent Memory Impairment. Arch Neurol, 50(9):967–973, 1993.

[115] James P Lister and Carol A Barnes. Neurobiological Changes in the Hippocampus During Normative Aging. Archives of Neurology, 66(7):829–833, 2009.

[116] J A Bernard, S J Peltier, J L Wiggins, S M Jaeggi, M Buschkuehl, B W Fling, Y Kwak, J Jonides, C S Monk, and R D Seidler. Disrupted cortico-cerebellar connectivity in older adults. Neuroimage, 83:103–119, 2013.

[117] H K Hausman, T B Jackson, J R M Goen, and J A Bernard. From Synchrony to Asynchrony: Cerebellar-Basal Ganglia Functional Circuits in Young and Older Adults. Cereb Cortex, 30:718–729, 2020.

[118] Kevin M Aquino, Ben Fulcher, Stuart Oldham, Linden Parkes, Leonardo Gollo, Gustavo Deco, and Alex Fornito. On the intersection between data quality and dynamical modelling of large-scale fMRI signals. bioRxiv, 2021.

[119] C Ahrends, A Stevner, U Pervaiz, M L Kringelbach, P Vuust, M Woolrich, and D Vidaurre. Data and model considerations for estimating time-varying functional connectivity in fMRI. bioRxiv, 2021.

[120] Fernando E Rosas, Pedro AM Mediano, Michael Gastpar, and Henrik J Jensen. Quantifying high-order interdependencies via multivariate extensions of the mutual information. Physical Review E, 100(3):032305, 2019.

[121] Giovanni Petri, Paul Expert, Federico Turkheimer, Robin Carhart-Harris, David Nutt, Peter J Hellyer, and Francesco Vaccarino. Homological scaffolds of brain functional networks. Journal of The Royal Society Interface, 11(101):20140873, 2014.

[122] Louis-David Lord, Paul Expert, Henrique M Fernandes, Giovanni Petri, Tim J Van Hartevelt, Francesco Vaccarino, Gustavo Deco, Federico Turkheimer, and Morten L Kringelbach. Insights into brain architectures from the homological scaffolds of functional connectivity networks. Frontiers in systems neuroscience, 10:85, 2016.

[123] Caleb Geniesse, Olaf Sporns, Giovanni Petri, and Manish Saggar. Generating dynamical neuroimaging spatiotemporal representations (DyNeuSR) using topological data analysis. Network Neuroscience, 3(3):763–778, 2019.

[124] Tamàs Fülöp, Mathieu Desroches, Alan A Cohen, Fernando Antônio Nóbrega Santos, and Serafim Rodrigues. Why we should use topological data analysis in ageing: Towards defining the "topological shape of ageing". Mechanisms of Ageing and Development, 2020.

[125] Anibal M Medina-Mardones, Fernando E Rosas, Sebastián E Rodríguez, and Rodrigo Cofré. Hyperharmonic analysis for the study of high-order information-theoretic signals. JPhys Complexity, 2021.

[126] Michael Wibral, Viola Priesemann, Jim W Kay, Joseph T Lizier, and William A Phillips. Partial information decomposition as a unified approach to the specification of neural goal functions. Brain and Cognition, 2017.

[127] Tycho M S Tax, Pedro A M Mediano, and Murray Shanahan. The partial information decomposition of generative neural network models. Entropy, 2017.

[128] Nihat Ay, Daniel Polani, and Nathaniel Virgo. Information decomposition based on cooperative game theory. arXiv preprint arXiv:1910.05979, 2019.

[129] Conor Finn and Joseph T Lizier. Generalised measures of multivariate information content. Entropy, 22(2):216, 2020.

[130] Fernando E Rosas, Pedro A M Mediano, Borzoo Rassouli, and Adam B Barrett. An operational information decomposition via synergistic disclosure. Journal of Physics A: Mathematical and Theoretical, 2020.

[131] Aaron J Gutknecht, Michael Wibral, and Abdullah Makkeh. Bits and pieces: Understanding information decomposition from part-whole relationships and formal logic. Proceedings of the Royal Society A, 477(2251):20210110, 2021.

[132] Kyle Schick-Poland, Abdullah Makkeh, Aaron J Gutknecht, Patricia Wollstadt, Anja Sturm, and Michael Wibral. A partial information decomposition for discrete and continuous variables. arXiv preprint arXiv:2106.12393, 2021.

[133] Klaas Enno Stephan, Nikolaus Weiskopf, Peter M Drysdale, Peter A Robinson, and Karl J Friston. Comparing hemodynamic models with dcm. Neuroimage, 38(3):387–401, 2007.

[134] World Health Organization. Dementia. `https://www.who.int/news-room/fact-sheets/detail/dementia`, 2021.

[135] Jennifer L. Whitwell, Scott A. Przybelski, Stephen D. Weigand, Robert J. Ivnik, Prashanthi Vemuri, Jeffrey L. Gunter, Matthew L. Senjem, Maria M. Shiung, Bradley F. Boeve, David S. Knopman, Joseph E. Parisi, Dennis W. Dickson, Ronald C. Petersen, Clifford R. Jack, and Keith A. Josephs. Distinct anatomical subtypes of the behavioural variant of frontotemporal dementia: A cluster analysis study. Brain, 2009.

[136] Federica Agosta, Elisa Canu, Lidia Sarro, Giancarlo Comi, and Massimo Filippi. Neuroimaging findings in frontotemporal lobar degeneration spectrum of disorders, 2012.

[137] Norman A.S. Farb, Cheryl L. Grady, Stephen Strother, David F. Tang-Wai, Mario Masellis, Sandra Black, Morris Freedman, Bruce G. Pollock, Karen L. Campbell, Lynn Hasher, and Tiffany W. Chow. Abnormal network connectivity in frontotemporal dementia: Evidence for prefrontal isolation. Cortex, 2013.

[138] Jennifer L. Whitwell and Keith A. Josephs. Recent advances in the imaging of frontotemporal dementia. Current Neurology and Neuroscience Reports, 2012.

[139] Katya Rascovsky, John R. Hodges, David Knopman, Mario F. Mendez, Joel H. Kramer, John Neuhaus, John C. Van Swieten, Harro Seelaar, Elise G.P. Dopper, Chiadi U. Onyike, Argye E. Hillis, Keith A. Josephs, Bradley F. Boeve, Andrew Kertesz, William W. Seeley, Katherine P. Rankin, Julene K. Johnson, Maria Luisa Gorno-Tempini, Howard Rosen, Caroline E. Prioleau-Latham, Albert Lee, Christopher M. Kipps, Patricia Lillo, Olivier Piguet, Jonathan D. Rohrer, Martin N. Rossor, Jason D. Warren, Nick C. Fox, Douglas Galasko, David P. Salmon, Sandra E. Black, Marsel Mesulam, Sandra Weintraub, Brad C. Dickerson, Janine Diehl-Schmid, Florence Pasquier, Vincent Deramecourt, Florence Lebert, Yolande Pijnenburg, Tiffany W. Chow, Facundo Manes, Jordan Grafman, Stefano F. Cappa, Morris Freedman, Murray Grossman, and Bruce L. Miller. Sensitivity of revised diagnostic criteria for the behavioural variant of frontotemporal dementia. Brain, 2011.

[140] M. L. Gorno-Tempini, A. E. Hillis, S. Weintraub, A. Kertesz, M. Mendez, S. F. Cappa, J. M. Ogar, J. D. Rohrer, S. Black, B. F. Boeve, F. Manes, N. F. Dronkers, R. Vandenberghe, K. Rascovsky, K. Patterson, B. L. Miller, D. S. Knopman, J. R. Hodges, M. M. Mesulam, and M. Grossman. Classification of primary progressive aphasia and its variants. Neurology, 2011.

[141] Juan Zhou, Michael D. Greicius, Efstathios D. Gennatas, Matthew E. Growdon, Jung Y. Jang, Gil D. Rabinovici, Joel H. Kramer, Michael Weiner, Bruce L. Miller, and William W. Seeley. Divergent network connectivity changes in behavioural variant frontotemporal dementia and Alzheimer's disease. Brain, 2010.

[142] Silvia P. Caminiti, Nicola Canessa, Chiara Cerami, Alessandra Dodich, Chiara Crespi, Sandro Iannaccone, Alessandra Marcone, Andrea Falini, and Stefano F. Cappa. Affective mentalizing and brain activity at rest in the behavioral variant of frontotemporal dementia. NeuroImage: Clinical, 2015.

[143] Rozita Jalilianhasanpour, Elham Beheshtian, Farzaneh Ghazi Sherbaf, Sadaf Sahraian, and Haris I. Sair. Functional Connectivity in Neurodegenerative Disorders: Alzheimer's Disease and Frontotemporal Dementia. 2019.

[144] Rahul S. Desikan, Florent Ségonne, Bruce Fischl, Brian T. Quinn, Bradford C. Dickerson, Deborah Blacker, Randy L. Buckner, Anders M. Dale, R. Paul

Maguire, Bradley T. Hyman, Marilyn S. Albert, and Ronald J. Killiany. An automated labeling system for subdividing the human cerebral cortex on MRI scans into gyral based regions of interest. NeuroImage, 2006.

[145] Stephen M. Smith and Thomas E. Nichols. Threshold-free cluster enhancement: Addressing problems of smoothing, threshold dependence and localisation in cluster inference. NeuroImage, 2009.

[146] Massimo Filippi, Federica Agosta, Elisa Scola, Elisa Canu, Giuseppe Magnani, Alessandra Marcone, Paola Valsasina, Francesca Caso, Massimiliano Copetti, Giancarlo Comi, Stefano F. Cappa, and Andrea Falini. Functional network connectivity in the behavioral variant of frontotemporal dementia. Cortex, 2013.

[147] Matthew D. Macfarlane, David Jakabek, Mark Walterfang, Susanna Vestberg, Dennis Velakoulis, Fiona A. Wilkes, Christer Nilsson, Danielle Van Westen, Jeffrey C.L. Looi, and Alexander Frizell Santillo. Striatal Atrophy in the Behavioural Variant of Frontotemporal Dementia: Correlation with Diagnosis, Negative Symptoms and Disease Severity. PLoS ONE, 2015.

[148] Dong Seok Yi, Maxime Bertoux, Eneida Mioshi, John R. Hodges, and Michael Hornberger. Fronto-striatal atrophy correlates of neuropsychiatric dysfunction in frontotemporal dementia (FTD) and Alzheimer's disease (AD). Dementia & Neuropsychologia, 2013.

[149] Maxime Bertoux, Claire O'Callaghan, Emma Flanagan, John R. Hodges, and Michael Hornberger. Fronto-striatal atrophy in behavioral variant frontotemporal dementia and alzheimer's disease. Frontiers in Neurology, 2015.

[150] Javier Rasero, Antonio Jimenez-Marin, Ibai Diez, Mazahir T Hasan, and Jesus M Cortes. Genes involved in cholesterol cascades are linked to brain connectivity in one third of autistic patients. bioRxiv, 2020.

[151] Marilyn Gatica, Fernando E Rosas, Pedro A M Mediano, Patricio Orio, Ibai Diez, Stephan P Swinnen, Rodrigo Cofre, and Jesus M Cortes. High-order functional interactions in ageing explained via alterations in the connectome in a whole-brain model. BioRxiv, 2021.

[152] Patricio Orio, Marilyn Gatica, Rubén Herzog, Jean Paul Maidana, Samy Castro, and Kesheng Xu. Chaos versus noise as drivers of multistability in neural networks. Chaos: An Interdisciplinary Journal of Nonlinear Science, 28(10):106321, 2018.

Introducción

Envejecimiento saludable y enfermedades cerebrales

Estudiar en envejecimiento desde la perspectiva de la neurociencia es de gran interés desde un punto de vista socioeconómico, dado que la cantidad de adultos mayores están aumentando considerablemente a lo largo del mundo. Las proyecciones sugieren que el porcentaje de personas sobre más de 60 años podría incrementar a 900 millones en el año 2015, y a 2.1 billones para el año 2050 [1, 2]. El envejecimiento es el mayor factor de riesgo para alteraciones cerebrales de alteración tardía, que aceleran el deterioro cognitivo y motor, y empeoran la calidad de vida.

Diversas causas del declinamiento sistémico subyacen al proceso del envejecimiento, involucrando efectos biológicos, cognitivos y fisiológicos. Por ejemplo, el envejecimiento altera los ritmos circadianos y ciclos de sueño [3], resultando en una pobre calidad del sueño, deteriora el rendimiento cognitivo, tal como la velocidad del procesamiento de información, memoria de trabajo, funciones ejecutivas y razonamiento [4], e inclusive aumenta los problemas de salud mental tales como ansiedad y depresión [5].

Adicionalmente, es importante por muchas razones caracterizar los cambios cognitivos subyacentes al envejecimiento de un cerebro sano, y distinguir entre la edad cronológica de un cerebro y la edad del cerebro estimada mediante los datos de resonancia magnética de pacientes. Primero, esto podría ayudar a tratamientos y cuidados específicos. Segundo, el envejecimiento es un considerable factor de riesgo para enfermedades neurodegenerativas que afectan a la cognición, tales como las enfermedades de Alzheimer y Parkinson. Afortunadamente, los avances en neuroimagen, preprocesamiento de datos y machine learning han contribuido sinérgicamente a tener mejores soluciones al problema de la predicción de edad [6]. Estos avances han llevado a un mejor entendimiento del proceso de envejecimiento de un cerebro sano, podrían motivar a nuevas intervenciones o prototipos de terapias que puedan contrarrestar los efectos neurodegenerativos o el deterioro producto del envejecimiento [7, 8, 9, 10, 11]..

Neuroimagen

Existen diversas técnicas no invasivas de neuroimagen para medir actividad cerebral en humanos. La imagen de resonancia magnética (MRI, por sus siglas en inglés) es una tecnología versátil para extraer información a gran escala tanto funcional como estructural de la organización cerebral. Existen diversos parámetros de adquisición de

la MRI, tales como la intensidad del campo magnético su dirección, su forma, y el número de secuencias de pulso para cambiar el gradiente del campo magnético o sus tiempos de relajación. Particularmente, la MRI estructural nos permite el estudio de tejidos anatómicos tales como la materia gris, blanca y fluido cerebroespinal (CSF) a lo largo de todo el cerebro, e incluyendo estructuras corticales y subcorticales, inclusive estructuras más internas como el tronco del encéfalo o el cuerpo estriado [12]. La imagen de resonancia magnética de difusión (dMRI, por sus siglas en inglés) nos permite rastrear el movimiento aleatorio tridimensional de las moléculas de agua en dichos tejidos. Esto es relevante porque, por ejemplo, en la materia gris y CSF, la difusión es altamente isotrópica, mientras que en la materia blanca la difusión de las moléculas de agua es anisotrópica, con algunas direcciones más visitadas que otras. Luego de diversas estrategias para reconstruir dichas trayectorias, dMRI proporciona un mapa de tractos de materia blanca que conectan pared de regiones a lo largo del cerebro completo, y a resolución de milímetros.

La imagen de resonancia magnética funcional (fMRI) es una técnica no invasiva descubierta en los años 90 por Seiji Ogawa [13]. Esta técnica se basa en las propiedades magnéticas de la sangre, en particular, en los ciclos de oxigenación y desoxigenación de la hemoglobina en la sangre. La principal hipótesis de la fMRI es que si de alguna forma el cerebro se encuentra envuelto en una tarea específica, demandará una actividad neuronal sostenida, lo que en consecuencia aumentará el consumo de oxígeno. De este modo, y muy importante, la fMRI es una medida indirecta de actividad neuronal.

Los avances de neuroimagen han evolucionado de la mano con la innovación y progreso en las metodologías y herramientas de preprocesamiento de imágenes [14, 15, 16, 17]. Existen diversos software y toolbox para pre-procesar y limpiar artefactos de distintas modalidades de MRI, tales como FSL, ANTs, MRtrix3, SPM, AFNI, por nombral algunos. Es importante mencionar que estas nuevas técnicas de neuroimagen y preprocesamiento, están llevando a grandes progresos en la investigación cualitativa clínica.

Otra técnica para medir actividad cerebral en el cerebro completo es la electroencefalografía (EEG) o magneto electroencefalografía (MEG), donde ambas se basan en las propiedades eléctricas y magnéticas de la excitabilidad celular de las células cerebrales. Aunque tanto la EEG como la MEG tienen una gran resolución temporal, e inclusive capaces de capturas variaciones de actividad neuronal en milisegundos, su resolución espacial es pobre. En esta tesis doctoral, nos enfocaremos solamente en dos modalidades de MRI, fMRI y dMRI.

Conectividad estructural

Cuantitativamente, se han descrito distintos efectos del envejecimiento en imágenes cerebrales estructurales. A lo largo del envejecimiento, el volumen total del cerebro aumenta desde la infancia hasta la adolescencia en aproximadamente un 25% en promedio,

luego permanece constante durante las siguientes tres décadas, y finalmente decae al tamaño de la infancia en edades más tardíass [18]. Adicionalmente, se ha mostrado que la atrofia en cerebros envejecidos no es homogénea, y algunas regiones anatómicas están más afectadas que otras: es bien sabido que dichas estructuras son el hipocampo [19], la corteza prefrontal [20] y los ganglios basales [21, 22]. La materia blanca se degenera más rápido que la materia gris a lo largo del envejecimiento, lo que indica que la conectividad total se ve disminuida con la edad [23]. Además, se ha mostrado un decrecimiento progresivo en diversas medidas de integridad de tractos utilizando imágenes de difusión, la cual es más pronunciada en sujetos sobre los 60 años de edad [7, 24].
El envejecimiento también ha sido estudiado en términos de mapas de conectividad de actividad neuronal, denominados conectividad estructural (SC). Diversos investigadores han caracterizado la SC a lo largo del envejecimiento, siguiendo las ideas seminales de integración y segregación propuestas por Tononi, Sporns y Edelman, proponiendo los conceptos de integración y segregación. La segregación le permite a las áreas cerebrales realizar tareas específicas de forma independiente. Mientras que la integración le permite a las áreas cerebrales trabajar de manera conjunta para efectuar tareas goal-directed [25, 26]. Siguiendo esta línea, diversos estudios han mostrado un decrecimiento de la segregación y un aumento de la integración a lo largo del envejecimiento [27, 28, 29]. Sin embargo, la relación entre los cambios en la estructura cerebral y su función causados por el envejecimiento, sigue siendo en gran parte desconocida [30, 31, 32, 24].

Conectividad funcional

Otra forma de cuantificar los cambios producidos por la edad son las interdependencias funcionales a pares. Las correlaciones funcionales entre dos señales temporales de actividad cerebral son cuantificadas típicamente mediante la Correlación de Pearson. Estas correlaciones se almacenan en una matriz denominada conectividad funcional (FC). Además, diversos estudios han ido más lejos y han analizado los cambios de la conectividad funcional a lo largo del tiempo [33, 34, 35, 36, 37, 38]. Estudios previos de la conectividad funcional, en estado de reposo, a lo largo del envejecimiento han mostrado que regiones dentro de la red neuronal por defecto (DMN) se vuelven menos conectados funcionalmente, con el paso de la edad [39, 8, 40, 32]. Adicionalmente, las redes fronto parietal, saliencia y red de atención dorsal también muestran un grado de deterioro con la edad, en términos de reducción de la conectividad dentro de la red [41, 42, 43, 39]. En contraste, la conectividad entre redes aumenta con la edad entre las redes DMN, somatosensorial, y frontoparietal. En conjunto, los antecedentes descritos sugieren una pérdida general de especificidad funcional o segregación a lo largo de los circuitos cerebrales [46]. Aunque ha existido un importante aumento en el entendimiento de los efectos del envejecimiento en la función cerebral, estos efectos son menos entendidos que los efectos en la conectividad estructural, los cuales muestran una

progresiva desconexión con la edad.

Interacciones de alto orden

Una importante limitación de las conectividades funcionales previamente descritas, es que su análisis está restringido a conectividad a pares, ignorando los posibles efectos de órdenes mayores llamados interacciones o interdependencias de alto orden. Las interdependencias de alto orden nos permiten caracterizar la organización de los patrones cerebrales, distinguiendo entre interacciones dominadas por redundancia o sinergia, las que juegan un rol crucial en la dinámica neuronal [47, 48, 49, 50, 51, 52]. La redundancia se puede entender como una extensión de la noción convencional de correlación entre más de dos variables, donde cada variable contiene una "copia" de la misma información compartida con las otras variables [53]. En contraste, la sinergia corresponde a las relaciones estadísticas que regulan el todo, pero no las partes [54, 55, 56]. La sinergia permite que coexistan tanto la interdependencia local con la cohesión global, una condición que es fundamental para las funciones cerebrales de alto orden, mientras que la redundancia, incluye situaciones altamente sincronizadas como el sueño profundo o convulsiones epilépticas, que harían que el cerebro fuese menos adecuado a dicha coexistencia [26, 57]. Un estudio pionero en las interdependencias de alto orden y el envejecimiento mostró cambios significativos en la sinergia y redundancia al nivel de interacción de tripletas [58], así como también la existencia de un rol redundante, la DMN. Sin embargo, los efectos del envejecimiento en interacciones más allá de tripletas siguen en gran medida inexplorados, hasta donde sabemos.

Hipótesis y objetivos

Hipótesis

"La redundancia y sinergia son marcadores informacionales que describen los cambios del envejecimiento de un cerebro sano. Más aún, las variaciones en la organización de dichas interacciones funcionales de alto orden pueden ser explicadas por los cambios de las redes anatómicas cerebrales, las cuales se degeneran con la edad. Las diferencias en sinergia y redundancia podrían diferencias cerebros sanos de cerebros con patologías neutodegenerativas. "

Objetivos

- Cuantificar los cambios cerebrales en las interdependencias funcionales de alto orden, en términos de redundancia y sinergia, utilizando datos de fMRI de participantes entre 10 a 80 años.

- Analizar si las variaciones en las interdependencias funcionales de alto orden pueden explicarse por los cambios en las redes anatómicas del cerebro a lo largo del envejecimiento, utilizando un modelo de cerebro completo del tipo Dynamic mean field (DMF).
- Cuantificar los cambios en las interacciones funcionales de alto orden producidas por la Demencia Frontotemporal.

Visión general de la tesis

Este trabajo está dividido en cinco capítulos:
C1. Introducción: Proporcionamos una visión general de la tesis Doctoral.
C2. Materiales y métodos: Introducimos las herramientas principales e ideas utilizadas en el desarrollo de esta tesis, incluyendo la metodología global utilizada en esta investigación. Relacionamos dichos métodos con la literatura en el área de investigación. Los siguientes tres capítulos tienen sus propios métodos.
C3. Interdependencias de alto orden en el cerebro envejecido: Investigamos cómo la organización informacional de alto orden del cerebro cambia con la edad. Hipotetizamos que la redundancia y sinergia son marcadores informacionales que describen los cambios en la actividad cerebral funcional de un cerebro sano durante el envejecimiento. Nuestros resultados muestran que los participantes mayores (de 60 a 80 años) exhiben una mayor predominancia de la redundancia que los sujetos más jóvenes. Este efecto se evidencia en todos los órdenes de interacción.
C4. Interdependencias de alto orden en un modelo de dinámica de cerebro completo: Combinamos datos de MRI funcional y estructural con un modelo de cerebro completo del tipo Dynamic mean field (DMF) para investigar los mecanismos subyacentes a los cambios del envejecimiento en la estructura e interacciones funcionales de alto orden. Hipotetizamos que las variaciones en los patrones funcionales pueden ser explicadas mediante los cambios en las redes anatómicas del cerebro, las cuales se degeneran con la edad. El modelo del tipo DMF reproduce con éxito que los sujetos mayores poseen una mayor redundancia que los sujetos más jóvenes, y para todo orden de interacción, reproduciendo así los resultados empíricos observados en el capítulo 3.
C5. Interdependencias de alto orden aplicadas a Demencia Frontotemporal: Analizamos las interacciones de alto orden en pacientes con Demencia Frontotemporal. Hipotetizamos que la redundancia y sinergia son marcadores informacionales que describen los cambios de actividad cerebral, producidos por la Demencia Frontotemporal. Nuestro tercer resultado muestra un clúster de tripletas con sinergia y redundancia desbalanceadas, y con algunas regiones participando de manera única en tripletas redundantes o sinérgicas.